Agro Waste Derived Activated Carbon as a Catalyst in Red-2G Degradation Process Optimized by Definitive Screening Design Approach

Fakhreddin, Mousavinia; Gholami, Ali*+

Department of Analytical Chemistry, Faculty of Chemistry, University of Kashan, Kashan, I.R. IRAN

ABSTRACT: *Red-2G is considered a non-biodegradable azo dye by United States environmental protection agency (EPA) as it is resistant against biological degradation. Here, a new method is presented to prepare activated carbon (ACP-850) using thermally treated pistachio nutshell and potassium oxalate as precursors to accelerate the dye degradation process with peroxymonosulfate (PMS) as oxidation agent. Having a high surface area (2318 m^2/g) and low-cost precursors, and the achievement of recyclable, biodegradable, and agricultural solid wastes are among the benefits of the proposed method. Also, the definitive-screening design approach is performed to evaluate the role of independent variables in degradation efficiency of PMS/ACP-850 system. Minitab response optimizer indicates the possibility of achieving a response value of 100% through the use of a factorial blend of PMS=3.0 mM, pH=3.0, ACP=1.0 g/L, and time= 80 min at room temperature for Red-2G concentration of 60 mg/L as optimum conditions. Furthermore, complete degradation of Red-2G with a higher concentration (170 mg/L) to H_2O and CO_2 as eco-friendly compounds occurs under following condition: PMS=6.0 mM, pH=3.0, ACP=2.0 g/L, and time= 180 min at a temperature of 55 °C,. Radical quenching experiments prove that sulfate anion radical ($SO_4^{-\bullet}$) and superoxide anion radical ($O_2^{\bullet-}$) play key roles as reactive species in the PMS/ACP-850 system at acidic and basic conditions, respectively. Reusability investigation confirms that ACP-850 can be frequently utilized to degrade dye from the contaminated solution. The LC/MS/MS and UV-VIS spectrometry analysis results along with mineralization rate demonstrate the effective possibility of decomposing Red-2G by the PMS/ACP-850 system.*

KEY WORDS: *Design of experiment; High surface area activated carbon; Peroxymonosulfate; Pistachio nutshell; Potassium oxalate; Red-2G.*

INTRODUCTION

One of the major sources of environmental pollution is considered to be from the textile industry. In this regard, azo dyes have been among the main pollutants existing in the textile sewage [1, 2]. Different kinds of dyes are utilized in textile industries due to different features such as unique color, resistivity and varying performance because of the divers functional groups in the dye molecules. Red- 2G (Acid Red 1) is an aryl azo naphthol compound (Figure 1), as included among eleven non-biodegradable azo dyes introduced by United States environmental protection agency (EPA) arising from its resistivity toward biological degradation by the activated sludge process [3, 4].

Azo dyes are decomposed to aliphatic and aromatic amines, acting as carcinogenic and mutagenic for living organisms [5]. Thus, structural stability and bio-toxicity of these organic dyes make it vital to develop eco-friendly approaches to reducing or degrading dyes and dyestuffs

**To whom correspondence should be addressed.*

+ E-mail: agholami@kashanu.ac.ir

1021-9986/2024/4/1691-1718 28/$/7.08

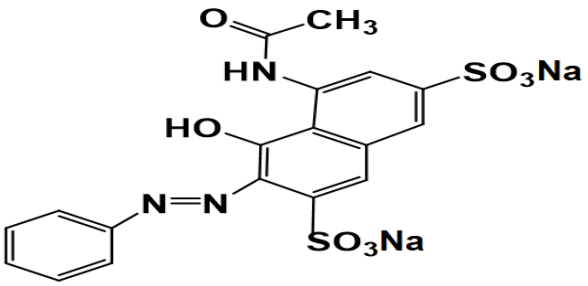

Fig 1: Red-2G

in various kinds of wastewater samples.

Advanced oxidation processes (AOPs) have been proposed to replace conventional industrial wastewater treatment, attracting considerable attention owing to their high degradation efficiency for resistant and bio-recalcitrant organic pollutions [6, 7], and their mechanisms are mainly related to the role of sulfate and hydroxyl radicals in the degradation process [8-12]. There are two approaches to accomplish AOPs: one is the in situ generation of radicals, and the other is the reaction of radicals with biological or organic pollutants [13]. These approaches are based on the utilization of different oxidant, catalyst and radiation such as photo catalysts [14-17], magnetic photocatalyst [18], TiO_2 [19-21],TiO_2 semiconductor with SnO_2 [22, 23], ZnO [24, 25], green nanocomposites such as Ni/Fe_3O_4@Nanocellulose[26] ozone [27, 28] hydrogen peroxide [29, 30], electro-peroxone process [31, 32], electrocatalytic degradation [33], peroxymonosulfate (PMS) or persulfate [7, 34-36], metal catalysts [37-40] or combination of ultraviolet (UV) radiation with other oxidants and catalysts [41-43].

Activated carbon as a kind of carbonaceous adsorbent has shown specific properties, including easy handling, large specific area and appropriate performance in the removal of dyes [44, 45]. In this regard, researchers have focused on them while some problems including the small removal efficiency, expensive reagents and disposal of toxic sludge materials restrict the applications of activated carbon. Accordingly, growing low-precursors for making activated carbon will be of higher effectiveness and favorability. In fact, carbonaceous-based materials (acting as green catalysts) decreased the application of other kinds of oxidant activator (e.g., expensive and toxic metals and metal oxides).

Pistachio nutshells (PNSs) are by-products of pistachios; being one of the popular nuts worldwide and belonging to the cashew family [46]. Pistachio can withstand harsh weather circumstances. Iran is one of the most important pistachio tree growing countries in the world as well as the first producer of this product in the Middle East and Asia. On the basis of previous statistics, the area under pistachio cultivation exceeds 300,000 hectares in Iran. At the moment, Iran is considered the main pistachios producer in the world. Therefore, the disposal of the waste materials extracted from processing and cultivation presents an important challenge annually [47]. In fact, around 30×10^6 tons of pistachio green shell are generally discharged as solid waste by-products materials [48].

In a previous work, crushed pistachio nut shell and potassium oxalate salt with less corrosiveness and easy controllability (acting as an activating reagent) were used to synthesize activated carbon at 800°C for 2 h under nitrogen purging with one variable at a time methodology [47]. Additional benefits of potassium oxalate are producing large surface area with a product yield of almost two times higher than that of KOH activator [49, 50]. The performance of the degradation process depends on many factors, so the study of the variable effects requires many experiments to be performed in the one variable at a time methodology as a conventional way [51, 52]. To prevail these conditions, one can utilize statistical design methods, including Doehlert, Box–Behnken and central composite rotatable designs, which are the most common approaches [53]. As a disadvantage, the number of experiments performed for the aforementioned methods will significantly increase by increasing the number of variables. When the number of variables exceeds five, one should utilize statistical screening methods in order to recognize the significant variables, whilst also deleting insignificant ones [54]. To this end, the two-level Plackett–Burman design has been vastly employed, although it is not capable of extracting pure-quadratic and interactive effects [55]. The three-level screening design is a assured way to solve the subject. In this case, Jones and Nachtsheim have been able to develop a three-level definitive screening design (DSD) for the first time [56]. Altogether, the usual sequence for implement of multivariate analysis approach through a DOE set-up needs the two following steps: firstly the screening, and secondly the optimization. Hence, a DSD presents the

combination of the both phases in one step, thus being more effective than standard screening designs such as Plackett–Burman and fractional factorial designs in order to detect non-linear interactions. According to the literature, some trials have been reported on the removal or elimination of Red-2G from aquatic systems [3, 57-59].

According to our experience, this design (DSD) has not been applied already for optimizing the degradation process, especially for Red-2G. Furthermore, most of the approaches employing the by-products of pistachio (e.g., shells, hulls, etc.) as adsorbents have utilized conventional methodologies [60-64].

This paper aims to focus on the production of ultra-high surface activated carbon using pistachio nut shell derived char as a helpful precursor and also potassium oxalate as activating agent. It is an effective simple catalyst in the Red-2G degradation process to H_2O and CO_2 through a novel approach of DSD [65]. This assures the protection of method greenness, requiring the lowest amount of materials and resources involved such as chemicals, energy, and test run.

MATERIALS AND METHODS

Materials, Apparatus and Software

All the reagents and chemicals used in the present study were of analytical grade without performing further purification. Potassium peroxymonosulfate (PMS; Oxone $KHSO_5 \cdot 0.5KHSO_4$ $0.5K_2SO_4$, $KHSO_5 \geq$ 47% w/w), tert-butyl alcohol ($C_4H_{10}O$, ≥ 99.5%), and potassium oxalate mono hydrate ($C_2K_2O_4.H_2O$, 99.5%) were obtained from Exir (Austria). Red-2G ($C_{18}H_{13}N_3Na_2O_8S_2$, ≥ 98), HCl (37%), ethanol (EtOH, ≥99.9%), and NaOH (≥ 99.0 %) were purchased from Merck. Sodium amide (NaN_3, ≥ 99.0 %) and p-benzoquinone ($C_6H_4O_2$, ≥ 98.0%) were purchased from Sigma Aldrich. The TOC reagent (Product number: 2760345) was purchased from HACH Company. To perform absorbance measurements, a UV-Vis spectrophotometer (HACH-DR6000) equipped with 20 mm glass cell was employed. The wavelength accuracy, wavelength resolution, and photometric accuracy were respectively as follows: ±1 nm, 0.1 nm, and 5 mAbs at 0.0 - 0.5 Abs. To prepare all the solutions in the present study, ultrapure water (18.2 MΩ·cm) was used from a water purification system (AquaMax- Basic 360 Series). To measure the weight of dyes and PMS, a Shimadzu analytical balance (AUW 220 D series) was employed. An electric muffle furnace (ADVANTEC-FUW232PA) was used to prepare PNS catalysts and an electric drying oven (ADVANTEC-DRA430DA) was utilized to dry them in the preparation step. A Perkin–Elmer GX spectrometer was used to record Fourier transform infrared (FT-IR) spectra. X-ray diffraction (XRD) measurements were performed by a powder diffractometer (Philips PW 1730, Netherlands) using Cu Kα radiation (λ=1.54 A°).

A scanning electron microscope (SEM, FEI, Quanta 200, USA) equipped with energy dispersive spectroscope (EDS, Element Silicone Drift, USA) was used to investigate the surface morphology of PNSs derived catalysts. The surface area, pore size distribution and volume of the PNSs were determined by a volumetric gas adsorption technique (Belsorp mini 2, Japan). To study thermal stability of the PNS samples, a thermal gravimetric analyzer (DSC-TGA, TA-Q600-USA) was used at a temperature range between 25 and 800 °C.

LC/MS/MS from Agilent (USA) was applied for identification of degradation fragments, as equipped with column C18 and Agilent G6410 Triple Quadrupole Mass Spectrometer. The following condition was utilized for the analysis: column temperature =25 °C, mobile phase (A=40 mM ammonium acetate with 2.5% acetonitrile, B= acetonitrile) using Negative ESI mode in Mass spectrometer. In order to construct the proposed design, Minitab®18 software was obtained from Minitab Inc., State College, PA, USA.

Proxymonosulfate as Oxidation Agent

Anipsitakis and Dionysiou have been able to present a new chemical oxidant for the decomposition of organic contaminants, according to the literature [66, 67]. Potassium salt of PMS is stabilized in the triple salt form ($2KHSO_5.KHSO_4.K_2SO_4$) under trade names of Oxone (Fig. 2) [68]. Physical properties of Oxone are described by following expressions: a white crystal, non-toxic, highly stable, inexpensive and easily soluble in water. PMS is rather stable in water solutions, maintaining 95% of active oxygen in 3 days [69].

As a derivate of H_2O_2, the PMS ion comprises one H-atom substituted by a SO_3 group. Also, as an oxidant, PMS has a redox potential of 1.82 V on the basis of Eq. (1) [70], allowing for moderate oxidation of certain organic contaminants.

Table 1: Screened Factors, Levels, and Responses Measured for Red-2G

Variables/Codes/Units	Lower Level (-1)	Middle Level (0)	Upper Level (+1)
PMS Concentration/A/(mM)	1.0	2.0	3.0
ACP dose/B/(g/L)	0.3	0.6	1.0
Red-2G Concentration/C/(mg/L)	10.0	30.0	60.0
pH/D/(pH unit)	3.0	7.0	10.5
Temperature/E/(°C)	25.0	40.0	55.0
Stirring Time /F/(min)	30.0	60.0	90.0
Response "Y"	%DE		

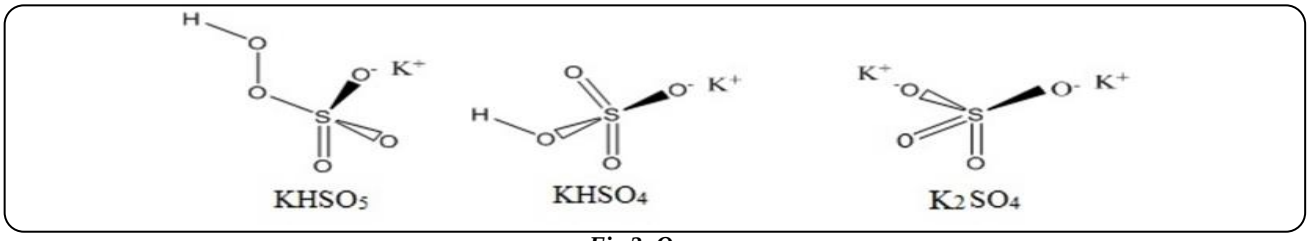

Fig 2: Oxone

$$HSO_5^- + 2H^+ + 2e^- \rightarrow HSO_4^- + H_2O \quad (1)$$

However, PMS is considered a strong oxidant from the thermodynamically aspect, so that the direct reaction of PMS with most pollutants is very slow. Therefore, the activation process is necessary and inevitable. Upon the activation PMS, the sulfate radical is produced, thereby playing a prominent role in the degradation of pollutants. In addition, the hydroxyl radical is another valuable product obtained from the activation of PMS. In the last decade, AOPs synthesized based on sulfate radicals have attracted consideration attention because of some of their unique properties. Sulfate anion radical ($SO_4^{\bullet-}$) is a strong oxidant, possessing a high oxidation potential of 2.5–3.1 V. It is possible to produce this radical by breaking the peroxo-bond of PMS material during its activation step [47, 71].

Preparation of the Activated Carbon from Pistachio nut Shells Derived Chars (ACP-850)

PNS-derived activated carbon was prepared at the temperature of 850 °C, whereas PNS derived chars to potassium oxalate ($C_2K_2O_4$) ratio was 1/2 and tested in decolorization of Red-2G. The powdery pistachio nutshells (mesh size of 35; equals to 500 microns) were carbonized at a temperature of 400 °C using a heating rate of 10 °C/min under N_2 atmosphere (150 ml/min) for 2 h, and the chars were activated in a platinum crucible with potassium oxalate (PNS derived char / $C_2K_2O_4$: 1/2) at 850 °C for 2 h. After cooling it down, a certain amount of chars was obtained from carbonization step, and $C_2K_2O_4$ as the activating reagent (W/W: 1/2) was mixed in the mortar and pestle as much as possible to produce a homogenous mixture. The mixture was then transferred to the crucible, followed by placing it in the furnace under N_2 purging (150 mL/min) at a temperature of 850 ºC for 2 h. Afterwards, under the N_2 purging, the mixture was cooled to 100 ºC. The resulting activated carbon (ACP-850) was then rinsed with deionized water until reaching pH of about 7.5. Ultimately, the rinsed samples dried in the oven at 100 ºC during 3 h.

Preparation of Adsorbate

The stock solution of Red-2G was obtained by dissolving precise amounts of the dye in ultrapure water for a final concentration equal to 100 ppm. The solutions with the desired concentrations were obtained using the same solvent, followed by adjusting the pH to certain values. Moreover, different concentrations of Red-2G were measured at 531 nm in order to obtain three calibration curves of Red-2G for the tested pH levels (lower, middle and upper levels), as presented in Table 1.

pH of Point of Zero Charge (pH_{PZC})

Measurement of pH point of zero charge (pH_{PZC}) for the produced activated carbon (ACP-850) was carried out by adding 0.1 g of activated carbon to NaCl solution (50 mL, 0.1 M)

Table 2: CHNS analysis data of raw PNS and ACP-850 with thermal treatment

Sample	C (%)	H (%)	N (%)	S (%)
PNS	41.75	5.63	2.96	0.13
ACP-850	69.04	0.68	2.46	0.00

with an initial pH adjusted to alter between 3-11 using NaOH or HCl solutions (0.1 M). The flasks were put on an agitator for 48 h after which the pH was measured with a constant temperature of 25 °C. For each sample, the pH was measured using a Seven Compact pH meter (Mettler Toledo, S220) [72].

Catalytic Degradation Test

To perform general degradation tests, conical flasks with a volume of 100 mL were used. Different conditions of the reacting solution such as temperature (25 °C, 40 ˚C, and 55 ˚C) and pressure (1 atm) were maintained constant in the entire tests. The oxidant (PMS) and dye (Red-2G stock solution) amounts were selected and added into the reactor, while also adjusting the pH via NaOH and HCl solutions. Next, by adding a certain ACP amount into the reaction mixture (containing dye and oxidant), the degradation processes continued while stirring the solution using a magnetic stirrer in order to obtain a homogeneous mixture. It should be noted that, by withdrawing about 2 mL of the sample, it was possible to determine the dye content immediately at the given reaction time intervals. The Red-2G degradation was monitored immediately using a maximum absorbance at the wavelength of 531 nm. The degradation efficiency was evaluated by DE% value as given in Eq. (2)[73, 74].

$$\text{Degradation Efficiency (DE)} = [(C_0\text{-}C_t)/C_0] \times 100 \quad (2)$$

where C_0 represents the initial Red-2G concentration (mg/L), and C_t denotes the concentration at time t for the PMS/ACP-850 system. The oxidation and mineralization of Red-2G were characterized by the chemical oxygen demand (COD) and total organic carbon (TOC) of reaction solutions for 1.5 and 24 h.

Desorption Studies

The ACP-850 (1 g/L) used for the sorption of 60 mg/L of Red-2G dye solution was filtered and dried. The sorbent was then agitated with distilled water (200 mL) at different pH values in the range between 2–12 during 24 h of the desorption process. Finally, the desorbed dye was measured.

Design of Experiments

As the factorial design, DSD was selected to perform the present investigation. In this respect, a single response i.e. the degradation efficiency (DE) was tried to be optimized as a function of six independent variables.

RESULTS AND DISCUSSION

Characterization and Properties of the ACP-850 Catalyst

Carbon, hydrogen, nitrogen, and sulfur (CHNS) analysis

The CHNS analysis results of PNS and the thermally activated derived catalyst (ACP-850) are presented in Table 2. The results show that the %C increases after the PNS thermal treatment because of converting it to the activated carbon (ACP-850). This can be ascribed to the thermal demolition of organic skeleton and further conversion into chiefly carbonaceous materials following the heat treatment process at 850 °C under nitrogen atmosphere.

However, the concentration of hydrogen atom is diminished from 5.63% in the PNS to 0.68% in ACP850. This phenomenon is explained by the simultaneous removal of hydrogen and oxygen as water loss with increase of the temperature. The PNS consisted of hemicelluloses, cellulose, and lignin as the main component. Also, some water and protein molecules may exist, so that the presence of nitrogen can be assigned to the content of the portein [75]. According to the report, the yield of CO, H_2O, H_2, CO_2, CH_4, C_2H_4, and C_2H_6 gases can be varied by changing the nature and temperature of the raw materials, resulting from the pyrolysis of cellulose, hemicellulose, and lignin materials [76]. Notably, upon the pyrolysis process, hemicelluloses generate more CO_2, whereas lignin mainly produces CH_4 and H_2.

SEM Micrographs

The surface morphology of powdery PNSs and activated carbon synthesized from pistachio shell (ACP-850) was carried out by using SEM. Fig. 3A shows the presence of small pores in the PNSs. By increasing the temperature in the ACP production process, the porosity increases as indicated in Fig. 3B. In fact, the number and size of the pores are enhanced.

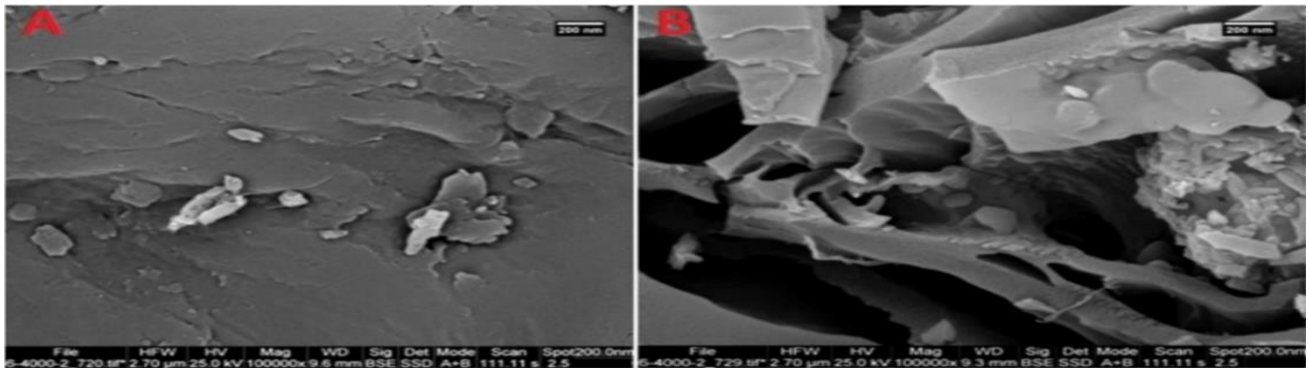

Fig 3: SEM micrographs: A) PNS B) ACP-850

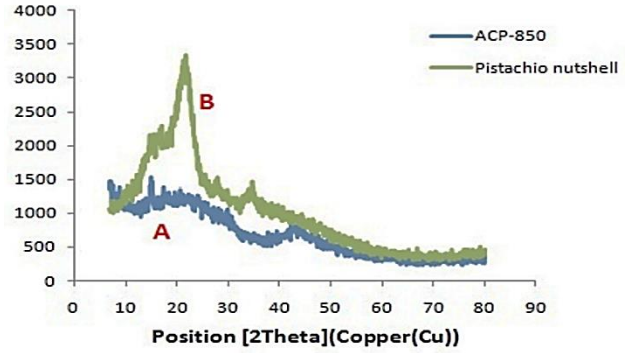

Fig 4: XRD patterns of (A) ACP-850, (B) Pistachio Shell

To synthesize porous carbon materials, chemical activation process has been employed vastly. In spite of physical activation, the conventional chemical activation involves the carbonization and activation in a single step process [77]. Compared to the physical activation, several advantages have been considered for the chemical activation such as higher yields and more extended pore structure [78], which can mainly be attributed to the activator penetrating deeply into the carbon lattice [79]. It is also stated that the porosity is enhanced at the higher temperatures (850 °C), arising from the conversion of aliphatic to aromatic compound [75]. As well, the decomposition of lignin, hemicelluloses and cellulose can be responsible for the free space of the cavities in the sample as major components. In other words, the pores created in the activated carbon can be assigned to the releasing of small molecules such as H_2O, CO_2, and CH_4H_2 from the texture at the high temperatures [75]. It is possible that oxidant and dye molecules can be trapped and degraded. As a matter of fact, the trapped process and dye degradation are facilitated by the porous structure and existence of cavities on the sample surface. The properties of the catalysts are chiefly determined by the pore structure, involving the shape, volume, average size, and size distribution of the pores. Also, the surface properties (e.g., the presence of functional groups and surface morphology) affect the catalysts' properties [80].

XRD Analysis

Fig. 4 shows XRD patterns obtained from PNS and ACP-850. As observed, cellulose is the main structural component of PNS. The sharp peak appeared at 2Theta=22.2º is related to the cellulose. In the case of ACP-850, the main peaks have lower intensity and become broader, being indicative of a less ordered structure. Accordingly, one can detect the broad and characteristic peak of the carbonaceous structure [81]. The peaks from the residual inorganic phases (e.g., calcite ($CaCO_3$) and halite (NaCl)) are observed in ACP-850, arising from the decomposition of organic phases at this temperature [82]. Similar patterns were also reported by other researchers who prepared activated carbons from agro-wastes [83, 84].

FT-IR Analysis

FT-IR spectral results of raw PNS and produced activated carbon (ACP-850) samples are given in Fig. 5. Spectrum of PNS demonstrates the existence of a broad characteristic band at 3426.16 cm^{-1} and a peak at 2904.44 cm^{-1}, which can be attributed to stretching vibrations of (-OH) and aliphatic C-H groups, respectively [85, 86]. Alternatively, ν(C=O) vibration in carbonyl group or the presence of carboxylic bonds on the surface is responsible for the appearance of the band at 1739.82 cm^{-1} for PNS [87, 88]. At higher temperatures, the intensity of these bands is reduced because of the degradation of carbonate compounds. Furthermore, the bands at 1626.84 cm^{-1} and 1509.08 cm^{-1} are

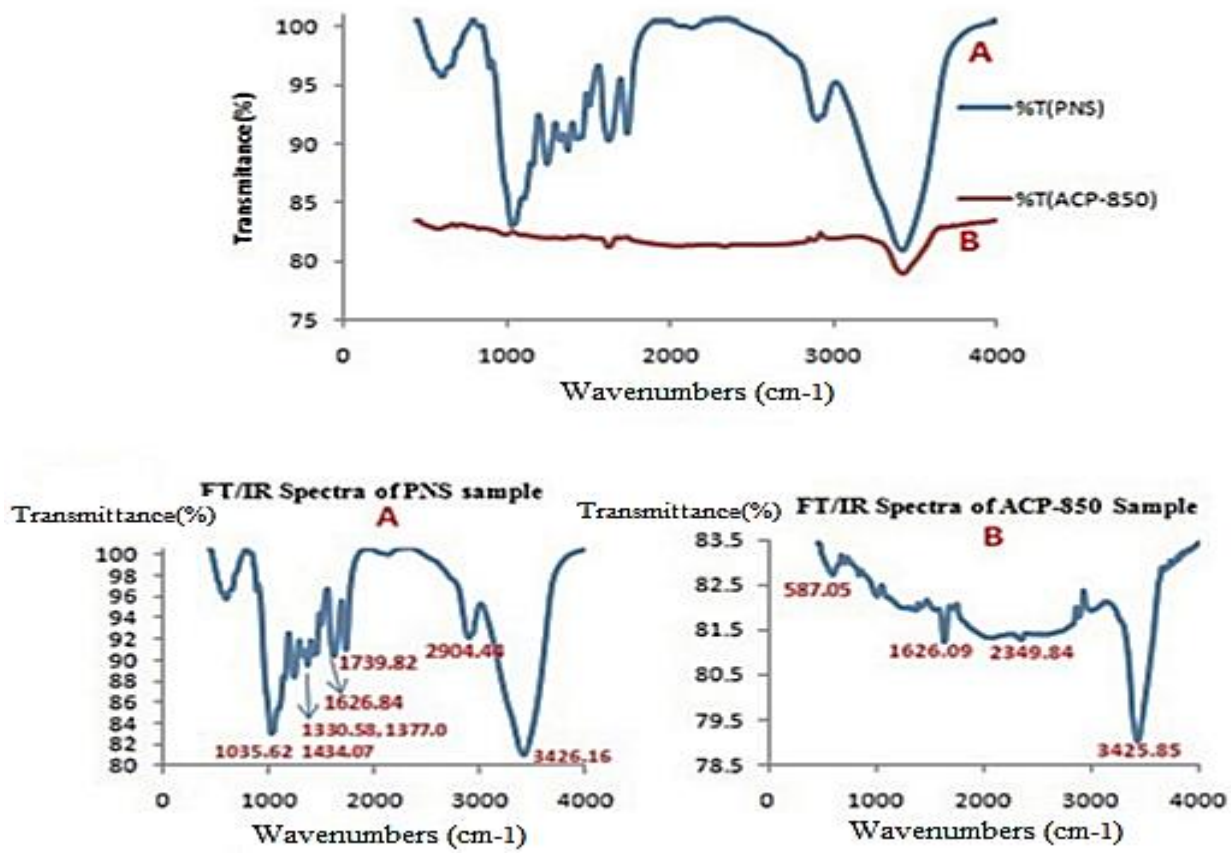

Fig 5: FTIR spectra of pistachio nutshell and obtained activated carbon at 850°C : A) PNS, B) ACP-850

attributed to the existence of aromatic C=O or C=C stretching of aromatic groups due to the lignin structure.

The sharp peak at 1035.62 cm^{-1} can be ascribed to the presence of C-O-C, being a specific peak in hemicelluloses and cellulose [64]. The bands at 1434.07, 1377.00 and 1330.58 cm^{-1} could be related to bending vibrations of O-H and C-H groups. Also, the spectrum of the obtained activated carbon (ACP-850) indicates slight moving of the position of some peaks compared to spectrum of pistachio nutshell. For instance, the bands at 3426.16 cm^{-1} and 1626.84 cm^{-1} in the PNSs are shifted to the new position at 3425.85 cm^{-1} and 1626.09 cm^{-1} in ACP-850, respectively. Moreover, the intensity of some peaks such as 3426.16 cm^{-1} in the spectrum decreases due to de-hydroxylation occurring during the pyrolysis process. As stated above, the bands appearing around 1626 cm^{-1} are assigned to C=O or C=C stretching of aromatic groups in lignin, indicating the presence of residual lignin after degradation. The pistachio nutshell is made of hemicelluloses, cellulose, and lignin as the main constituents. Accordingly, the elimination of hydroxyl, carbonyl, carboxylic and carbonate groups can be expected to occur in the form of water, CO_2, CO and small volatile organic compounds, arising from the thermal activation.

TGA Analysis

TGA results of PNS were obtained using N_2 atmosphere and a heating rate of 10 °C/min. From Fig. 6, the weight loss of the PNS sample is observed to occur through three major steps: At the first step, the sample loses the adsorbed water molecules from the surface in the temperature range between 25 and 100 C, followed by losing crystalline water around 200 °C. The weight loss of this step does not exceed 6.25 %. If the pistachio was purchased as non-roasted without any heat treatment prior to packing, the weight loss had increased. At the second step, more than 60% of the sample is disintegrated in the range of 200–400 ºC, and the two main peaks at 299.80 ºC and 346.81 ºC are distinguishable, being typical for pyrolysis of lignocelluloses materials [89]. Due to decomposition and carbonization of the organic materials existing in PNSs (hemicelluloses, cellulose, and lignin), the aforementioned sharp peaks appear in this

Table 3: BET Analysis Results of PNS and ACP-850 Samples

Parameters	PNS	ACP-850
BET Surface Area(m2/g)	1.0055	2318
Langmuir Surface Area(m2/g)	1.7212	2789
Total Pore Volume(cm3/g)	0.0101	1.1111

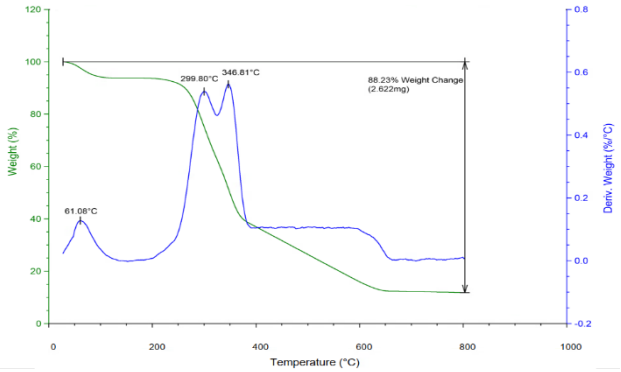

Fig 6: TGA Graph Of Pistachio Nutshell (PNS) at the Temperature Range of 25–800°C

temperature range. On the other hand, the peaks at 299.80 °C and 346.81 °C are generated due to degradation of hemicelluloses and cellulose present in the sample, respectively. The third step occurs between 400 °C and 700 °C, representing about 20% weight loss. Since lignin is more thermostable than cellulose and hemicelluloses, the above-mentioned temperature range is expressed for lignin decomposition. As shown in Fig. S3, the total weight loss is 88.23% prior the temperature range of 25-800 °C.

BET Analysis

Fig. 7 shows the adsorption-desorption isotherms of raw powdery pistachio nutshell (A) and obtained activated carbon (B) samples. The ACP-850 was prepared at 850 °C. Fig. 7-A indicates a type III isotherm, which is related to non-porous material such as raw PNS. At low relative pressures, a sharp increment (more than 600 cm^3g^{-1}) is observed in the adsorption–desorption isotherms, as shown in Fig. 7-B. This is followed by a plateau at higher relative pressures, demonstrating a type I isotherm according to IUPAC categorization. The type I isotherm indicates a material with microporous structure. The utilization of materials with highly porous structure and narrow pore size distribution leads to significant uptake at low relative pressures.

The micropore filling is represented by the initial part of the isotherm, and multilayer adsorption on the external surface is indicated by a low slope of the plateau [90]. The surface area of PNS and obtained activated carbon(ACP-850) was measured as given in Table 3.The results show that su rfaceareaincreases from 1.006 to 2318 m^2/g. The considerable increment in the surface area could be ascribed to the thermal and thermo-chemical treatment processes. In addition, the total volume of pores is enhanced from 0.010 to 1.111cm^3/g for PNS and ACP850 samples, respectively.

Definitive Screening Design (DSD)

As stated before, the aim of this study is to recycle PNS (as an agricultural byproduct) into the green catalyst with appropriate competency, which could be realized based on the utilization of the factorial design as an effective approach. In fact, DSD uses a screening design without the requirement of a further process for the optimization phase, involving a three-level design so that the number of runs produced is proportional to the number of variables (k) on the basis of the following relation: N = 2k + 1 or 2k + 3. Table 4 presents the experiment runs obtained from the factorial combinations of the design matrix and considering the two blocks [56, 65, 91]. DSD can act as a design in order to estimate the main effects, factorial interactions and quadratic effects provided by the lowest number of experiment runs. Obviously, DSD is advantageous for optimizing the processes that comprise a large number of operating variables. Herein, one response (i.e., degradation efficiency: (DE)) was taken into consideration for the present investigation. The goal was to maximize DE to 100%. Table 4 presents the design matrix, involving 13 basic runs in two replicates. Therefore, the total number of runs is 26 with two central points. The runs were operated in two blocks. In fact, the blocks were contained in order to establish the full quadratic model.

Data analysis and Modeling

The quadratic equation, (Eq. (3))[92] was used for data modeling preparation by each response.

Table 4: Design Matrix Along with the Responses Obtained from Observation and Prediction

Run	Coded Levels of Variables						Response (Y, Degradation Efficiency, DE)		
	A[1]	B[2]	C[3]	D[4]	E[5]	F[6]	Obs	** Pred.	*** %Er
01	0	0	0	0	0	0	80.24	80.60	0.45
02	-1	-1	0	-1	+1	+1	72.03	71.82	0.29
03	+1	-1	+1	0	+1	-1	52.36	52.53	0.32
04	0	+1	+1	+1	+1	+1	90.42	90.71	0.32
05	-1	+1	+1	-1	0	-1	45.50	45.35	0.33
06	+1	-1	-1	+1	0	+1	99.83	99.92	0.09
07	0	-1	-1	-1	-1	-1	68.23	68.06	0.25
08	-1	+1	-1	0	-1	+1	97.80	98.26	0.47
09	+1	+1	-1	-1	+1	0	99.83	99.46	0.37
10	-1	0	-1	+1	+1	-1	74.47	74.72	0.34
11	-1	-1	+1	+1	-1	0	20.45	20.57	0.59
12	+1	+1	0	+1	-1	-1	89.63	90.06	0.48
13	+1	0	+1	-1	-1	+1	97.00	96.63	0.38
14	+1	-1	+1	0	+1	-1	52.70	52.54	0.30
15	-1	0	-1	+1	+1	-1	75.00	74.72	0.37
16	+1	0	+1	-1	-1	+1	96.30	96.64	0.35
17	-1	-1	0	-1	+1	+1	71.58	71.82	0.34
18	0	0	0	0	0	0	81.00	80.60	0.49
19	-1	+1	-1	0	-1	+1	98.70	98.26	0.45
20	0	+1	+1	+1	+1	+1	91.00	90.71	0.32
21	-1	+1	+1	-1	0	-1	45.20	45.35	0.33
22	-1	-1	+1	+1	-1	0	20.70	20.57	0.63
23	+1	+1	0	+1	-1	-1	90.45	90.06	0.43
24	0	-1	-1	-1	-1	-1	67.88	68.06	0.27
25	+1	+1	-1	-1	+1	0	99.10	99.46	0.36
26	+1	-1	-1	+1	0	+1	100.00	99.92	0.08

[1,2, 3, 4,5,6] A, B, C, D,E, and F are defined in the upper section of Table 2. * Obs.: Experimental values,** Pred.: Predicted values *** %Er: % of prediction error = |(Obs - Pred.)|/Obs × 100.

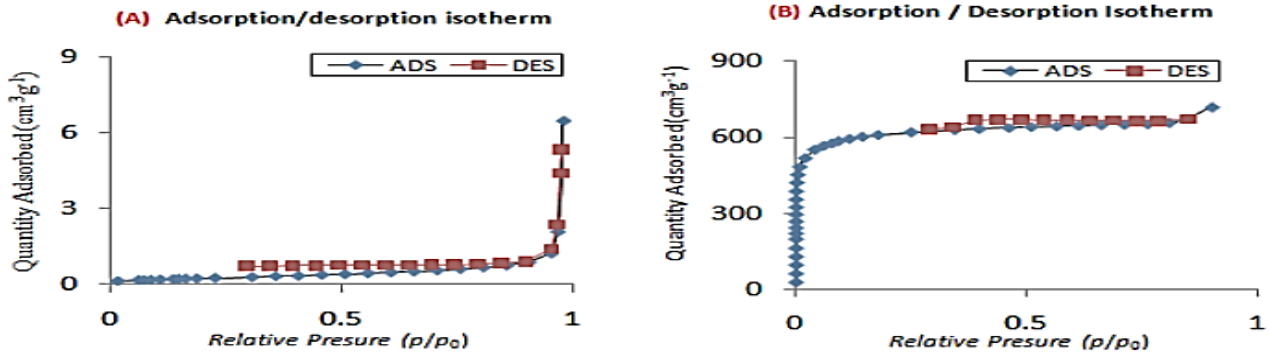

Fig 7: N2 Adsorption-Desorption Isotherms at 77 ° K for: A) PNS, B)ACP-850

$Y= b_0 + b_1X_1+b_2X_2 + ... + b_nX_n +\Sigma b_{ik}X_iX_k +\Sigma b_{ii}X_i^2$ (3)

where Y gives the measured responses, and b_0, b_1, etc. represent the regression coefficients (b_0 is a constant). X_i denotes an independent variable (A, B, C,…., F).

Moreover, X_iX_k and X_i^2 represent interaction and quadratic terms, respectively. The probability plot of the results showed that they were fitted in the normal distribution plot (P-value > 0.250). If the p-value is larger than the significance level (i.e., P-value= 0.05), the null hypothesis can still be considered valid because there is not enough evidence to conclude that the data distribution is not normal. The regression equation, (Eq. (4)), was obtained by DSD analysis section in the Minitab software using stepwise selection of full quadratic terms [92, 93].

$$\begin{aligned}\text{Response (DE)} = {} & 80.601 + 12.7885(\text{PMS}) \\ & + 11.0935(\text{ACP}) - 13.4605\ (\text{Red} \\ & - 2\text{G}) - 0.5350\ (\text{PH}) \\ & + 1.5675\ (\text{TEMPRATURE}) \\ & + 12.6620\ (\text{TIME}) - 5.911\ (\text{PH} \\ & * \text{PH}) + 1.006\ (\text{PMS} * \text{ACP}) \\ & + 5.744\ (\text{PMS} * \text{RED} - 2\text{G}) \\ & - 5.244(\text{PMS} * \text{TEMPRATURE}) \\ & + 4.694\ (\text{ACP} * \text{RED} - 2\text{G})\end{aligned}$$

$$R^2 = 99.98\%,\ R^2\text{-Adj} = 99.97\ \%,\ R^2\text{-Pred.} = 99.95\% \quad (4)$$

As can be inferred, the coefficient of determination value (R^2) is high, indicating the goodness-of-fit. In addition, the value of R^2-Adj is close to that of R^2-Pred, implicating the sufficiency of the proposed model to estimate the response for any new observation. There is very little difference between value of R^2-Pred and R^2, showing that the model is not over-fit. The values for the measured response predicted by the model are presented in Table 4. The percentage of prediction error (%Er) is found to be between 0.08–0.63%, which is relatively small (less than 1%), and demonstrates that the proposed model has appropriate efficiency for predicting the results [94-96].

Pareto Chart: Variables and the Interactions

The Pareto chart of the standardized effects was performed using variance analysis (ANOVA) at 95.0% confidence interval (95.0 CI) in order to evidence statistical significance of the tested independent variables, as mentioned in Table 1. As shown in Fig. 8; Pareto chart indicates that Red-2G concentration, PMS dosage, Time and ACP dosage as catalyst, are the main variables with high effects on the response, whereas the temperature and pH have lower effects compared to the other factors. As expected and shown by the Pareto chart, the PMS (A) and ACP dosages (B) [97] have the main role in the degradation efficiency as oxidant and activator, respectively. Table 4 indicates that the presence of PMS (A) induces the creation of reactive oxygen species, and different effects are obtained on the removal rate of dye contaminant depending on the PMS concentration, owing to the different conditions between each runs. Many research studies have indicated that the degradation rate of pollutants increases with increasing the concentration of PMS. However, it decreases when the PMS concentration reaches a certain level. While the addition of PMS can induce more oxidants (thus leading to an improvement in the contaminant removal efficiency), an excessive amount of PMS may result in its self-quenching reactions, thereby decreasing the degradation efficiency [98, 99] The concentration of ACP also plays an important role in the activation of PMS. This is because increasing the concentration of ACP (acting as a catalyst) not only increases the active sites in the PMS activation, but also enhances the reaction chance with dye molecules. Additionally, increasing the catalyst concentration leads to the creation of radicals, promoting the degradation of Red-2G [100].

Also, the following interactions can be presented by Pareto chart as effective interactions: (PMS × Red-2G concentration), (PMS × Temperature), (ACP × Red-2G concentration), (pH × pH) and (PMS × ACP). The amount and direction of the effect for each tested variable and related interactions can be found from the regression equation (Eq. (4)). As presented in Eq. (4), PMS, Time, ACP and Temperature (with a lower effect) have a positive effect on degradation efficiency, whereas the Red-2G and pH parameters negatively influence the degradation efficiency as the response. In other words, by increasing the Red-2G concentration and pH, the response will decrease at a specified rate for the aforementioned variables. As mentioned above and indicated by Pareto chart, dye concentration (C) has the highest impact with negative direction on the response, followed by two interactions with PMS (A) as degradation agent (AC interaction) and ACP dosage(B) as PMS activator (BC interaction), respectively. Therefore, the amount of the AC and BC interactions is affected by the negative effect of dye concentration factor (C), although they change the degradation efficiency in the positive direction as represented by the regression equation.

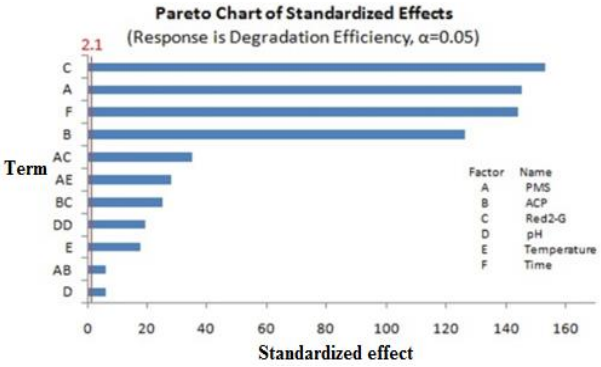

Fig 8: Pareto Chart of Standardized Effects. Degradation Efficiency (DE%) is the Measured Response. Variable Exceeding Reference Line (Red Line) are Statistically Significant

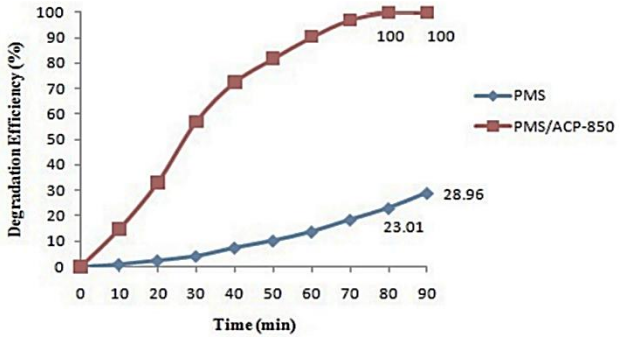

Fig 9: Catalytic effect of ACP-850 on Red-2G degradation: pure PMS and (PMS+ACP-850)
[Red-2G]$_o$= 0.12mM (60mg/l), [ACP-850]= 1.0 g/L, [PMS]= 3.0 mM, pH=3.0, T= 25 °C

One of the most influential factors that can change the PMS activation is the reaction temperature. This factor can also affect the subsequent degradation of contaminants. It is obvious that the removal rate of contaminants is improved by increasing the reaction temperature within a certain range. As well, the stability of PMS is affected by the temperature, so that the PMS decomposition to the related free radicals will be accelerated at a high temperature [101]. Based on the Pareto chart, temperature is contributed in the present study by two paths: Temperature itself with a positive affect (E) and given magnitude, and interaction of PMS × Temperature (AE) with a negative impact but greater intensity compared to the temperature factor. One of the important factors for activating the persulfate (PS) and PMS is the heat agent in degradation systems.

It has been estimated that the bond energy of O-O is 213.3 kJ/mol for PMS. The effective mechanism involved in the activation of PMS is the fission of O-O bond in its structure. In the case of heat activation, the energy input provided at the high temperature (>50 °C) leads to the fission of O-O bond, thereby forming sulfate anion radicals and hydroxyl radicals as given in Eq. (5) [34].

$$HSO_5^- \rightarrow SO4^{-\bullet} + HO^{\bullet} \quad (5)$$

The molecular movement will be accelerated by an increase in the temperature, thereby promoting the mass transfer process in heterogeneous systems. Consequently, the enhanced degradation rate of contaminants induced by the increase of temperature in a reasonable range is reliable, as previously evidenced in the literature [102, 103]

However, the side reactions such as hydroxyl radicals or recombination of sulfate radicals may be accelerated by the increase in temperature, leading to a reduction in the removal efficiency of the contaminants under test [104].

The interaction between PMS (A) and ACP (B) is shown by the Pareto chart (AB) with the positive direction and impact as indicated in the regression equation. As described above, because of the opposite directions of Red-2G variable (C) with the negative effect and ACP variable (B) with the positive effect in the present degradation system, positive interaction is produced between Red-2G molecules and ACP catalyst (BC). Therefore it can be stated that the right magnitude of the PMS×ACP interaction (AB) is affected by BC interaction in the Pareto chart system.

As shown in Fig. 9, it can be seen that Red-2G removal rate is negligible in PMS system alone, being attributable to the small oxidation potential (E° (HSO_5^-/HSO_4^-) = +1.82 V vs. NHE). From an applicable point of view, it appears that the activation of PMS in degradation systems is necessary due to its low reactivity (28.96%). Noticeably, the occurrence of a synergistic effect in the PMS/ACP degradation system caused ACP to donate an electron to PMS, thus creating the reactive radical and anion radical as given in Eqs. 6 and 7, and initiating the destructive reactions [7]. Based on Eq. 8, ACP-850 can also be used as an electron acceptor in the activation process of PMS. The adsorption of PMS and Red-2G was provided by the active and defective sites. Furthermore, the electron transfer from carbon materials to PMS was mediated by the partially delocalized π electrons, thereby allowing for the activation of PMS [103]. According to Ref. [99],

defective sites, carbon-conjugated structure, and appropriate amounts of functional groups are responsible for the persulfate activation capability of carbon materials [105].

$$HSO_5^- + \text{ACP} \rightarrow SO_4^{-\bullet} + \text{HO}^- + ACP^+ \quad (6)$$

$$HSO_5^- + \text{ACP} \rightarrow SO_4^{2-} + \text{HO}^\bullet + ACP^+ \quad (7)$$

$$HSO_5^- + ACP^+ \rightarrow SO_5^{-\bullet} + \text{H}^+ + \text{ACP} \quad (8)$$

Initially, ACP-850 approaches PMS, followed by adsorbing it on the surface. As described in Ref. [101], the defect structures of ACP-850 (e.g., edge defects, vacancies, curvature, etc.) can then create dangling σ bonds, thereby preventing the limitation of the π-electrons of activated carbon caused by the edge carbon atoms, and transferring electrons from activated carbon to PMS in order to generate $SO_4^{\bullet-}$ and $^\bullet$OH. Moreover, the transfer of lone pair of electrons in the Lewis basic site of the activated carbon-based catalysts (e.g., the O atom in C = O and the free flowing π-electrons in the sp^2-hybridized carbon) to PMS can be possible, thus inducing the generation of $SO_4^{\bullet-}$ and $^\bullet$OH [100].

Lastly, the pH variable is affected by the above-mentioned reactions with accompaniment of pH×pH interaction, indicating the presence of linear and nonlinear effects of the pH. It should be noted that the linear effect is less than the nonlinear (curve) effect, which is explained for three reasons as follows: Firstly, the pH is considered an important factor that controls the efficiency of dye removal from the experimental solution. Especially, dye molecules possess a pH-dependent structure [106, 107]. It means that the pH has a great influence on the speciation of dye molecules (e.g., Red-2G), affecting the reactivity toward an oxidation. Generally, the reactivity of pollutants such as dye molecules is enhanced by increasing the degree of their deprotonation. Secondly, pH plays an important role in the activation of PMS, thus further influencing the degradation efficiency of Red-2G. The existence form of PMS can be significantly changed by the pH of the solution. In general, PMS has a vast pH range of application, although the oxidation potential is affected by the pH.

Thirdly, pH has a significant influence on the heterogeneous activation of PMS as well. The ACP-850 surface is ionized to carry a positive charge at the low value of pH. On the other hand, it is important to determine the pH of point of zero charge of ACP-850 related to the pH at which the number of negative and positive charges is equal. At this pH point, an electrically neutral charged activated carbon is achieved. Accordingly, this is an essential factor to be noticed in the adsorption investigation, providing insights into the adsorption behavior of the surface of the activated carbon as a function of pH. The adsorption of anionic dyes such as Red-2G is suited when the pH of the solution is less than the pH_{PZC}. This is because the surface of the catalyst becomes positively charged and can be described by the electrostatic attraction between the positive charge (produced on the solid surface) and the anionic group of the Red-2G dye. The pH_{PZC} taken from the final pH as a function of the initial pH curve for the ACP-850 is presented in Fig. S1. Thus, the Red-2G dye can be adsorbed when the pH of the solution is less than the pH_{PZC} of the adsorbent, which is determined to be 7.1 based on Fig. S1 [108].Therefore, the considerable enhancement in the electrostatic interactions causes the adsorption capacity to increase for anionic Red-2G. On the other hand, Red-2G carries both negative and positive charges to generate an intermolecular salt, leading to the diminishment of hydration between Red-2G and water molecules, and significantly absorbing Red-2Gs on the surface of the ACP-850. Moreover, electrostatic repulsions between the negatively charged surface and the dye molecules are enhanced by an increase in the pH, so that the degradation mostly occurs in the bulk of the solution via alkaline activation which is in competition with the present degradation system. For the alkaline activation of peroxymonosuflate, the following mechanisms and reaction pathways can be expressed as given in Eqs. 9- 19.[109].

$$HSO_5^- + \text{H2O} \rightarrow H_2O_2 + HSO_4^- \quad (9)$$

$$HSO_5^- \rightarrow H^+ + SO_5^{2-} \quad (10)$$

$$SO_5^{2-} + \text{H2O} \rightarrow H_2O_2 + SO_4^{2-} \quad (11)$$

$$H_2O_2 \rightarrow H^+ + HO_2^- \quad (12)$$

$$H_2O_2 + \text{HO}^- \rightarrow \text{H2O} + HO_2^- \quad (13)$$

$$HSO_5^- + HO_2^- \rightarrow \text{H2O} + SO_4^{-\bullet} + {}^1O2 \quad (14)$$

$$H_2O_2 \rightarrow 2\text{HO}^\bullet \quad (15)$$

$$\text{HO}^\bullet + H_2O_2 \rightarrow \text{H2O} + HO_2^\bullet \quad (16)$$

$$HO_2^\bullet \rightarrow H^+ + O_2^{\bullet-} \quad (17)$$

$$\text{HO}^\bullet + O_2^{\bullet-} \rightarrow {}^1O2 + \text{HO}^- \quad (18)$$

$$2O_2^{\bullet-} + 2H^+ \rightarrow {}^1O2 + H_2O_2 \quad (19)$$

Table 5: Variance analysis (ANOVA) for the response data

Source	DF*	Adj SS*	Adj MS*	F-Value	P-Value
Model	11	14246.7	1295.15	8376.96	0.000
Linear	6	12617.3	2102.89	13601.32	0.000
PMS	1	3270.9	3270.91	21156.05	0.000
ACP	1	2461.3	2461.31	15919.61	0.000
RED-2G	1	3623.7	3623.70	23437.85	0.000
pH	1	5.7	5.72	37.03	0.000
Temperature	1	49.1	49.14	317.84	0.000
TIME	1	3206.5	3206.52	20739.58	0.000
Square	1	58.8	58.77	380.10	0.000
pH×pH	1	58.8	58.77	380.10	0.000
2-Way Interactions	4	1620.3	405.07	2619.96	0.000
PMS×ACP	1	5.8	5.83	37.68	0.000
PMS×RED-2G	1	189.8	189.85	1227.92	0.000
PMS×Temperature	1	122.3	122.32	791.14	0.000
ACP×RED-2G	1	98.0	98.01	633.90	0.000
Regression	1	14246.7	14246.7	157965.58	0.000
Error	24	2.2	0.1		
Lack of Fit	11	0.0	0.0	0.00	1.000
Pure Error	13	2.2	0.2		
Total	25	14248.9			

* DF: Degrees of Freedom; Adj SS: Adjusted sums of squares; and Adj MS: Adjusted mean of squares.

During the degradation of azo dyes (e.g., acid orange 7) and Red-2G with the same structure, singlet oxygen ($^1O2$) and superoxide radical were found to be the primary reactive species [34]. In addition to the above-mentioned reaction pathways, $^1O2$ can also be created by the self-decomposition reaction as given below [110]:

$$HSO_5^- + SO_5^{2-} \rightarrow HSO_4^- + SO_4^{-\bullet} + {}^1O2 \qquad (20)$$

According to the data presented in Table 2 and explanations about the pH factor provided above, high degradation efficiency at acidic and basic conditions together with considering the existing effects of the other variables leads us to the conclusion that the effect of the pH factor is moderate compared to the other effective variables.

ANOVA

Residual plots were applied to the experiment data of residual distribution. Normally, the residuals are independent of each other and distributed with a constant variance. Similar results were acquired based on the ANOVA testing, according to Table 5. It was possible to confirm the statistical significance of tested variables at confidence interval of 95.0% by achieving p-values less than 0.05. As well, it is found that F-statistic is relatively large for the model (see Table 5). While statistical significance of the tested variables is indicated by the linear, square and two-way interactions, the F-value is small in the case of pH (37.03), PMS×ACP interaction (37.68) based on the previous relevant description. Alternatively, F-value of lack-of-fit is zero whereas its p-value is equal to 1.000, showing that the proposed model suitably explains the relation between the response and the predictors.

Response Surface Optimization

Contour plots (also known as level plots) are an approach to demonstrating a three dimensional (3D) surface on a 2D plane. In this study, contour plots obtained from the response surface were accomplished to express the relationship existing between the measured response and independent variables, thereby allowing for the measurement of the efficacy of two variables while keeping the other variables constant at the same time. Fig. 10

Table 6: The Comparison between the Optimum and Maximum Performance of the Red-2G Degradation System

Study	PMS Concentration	ACP dose	Red-2G Concentration	pH	Temperature	Stirring Time	Degradation Efficiency(%)
Optimum Performance	3 mM	1.0 g/L	60 mg/L	3.0	25°C	80 min	100
Maximum	6 mM	2.0 g/L	170.15 mg/L	3.0	55°C	180 min	100

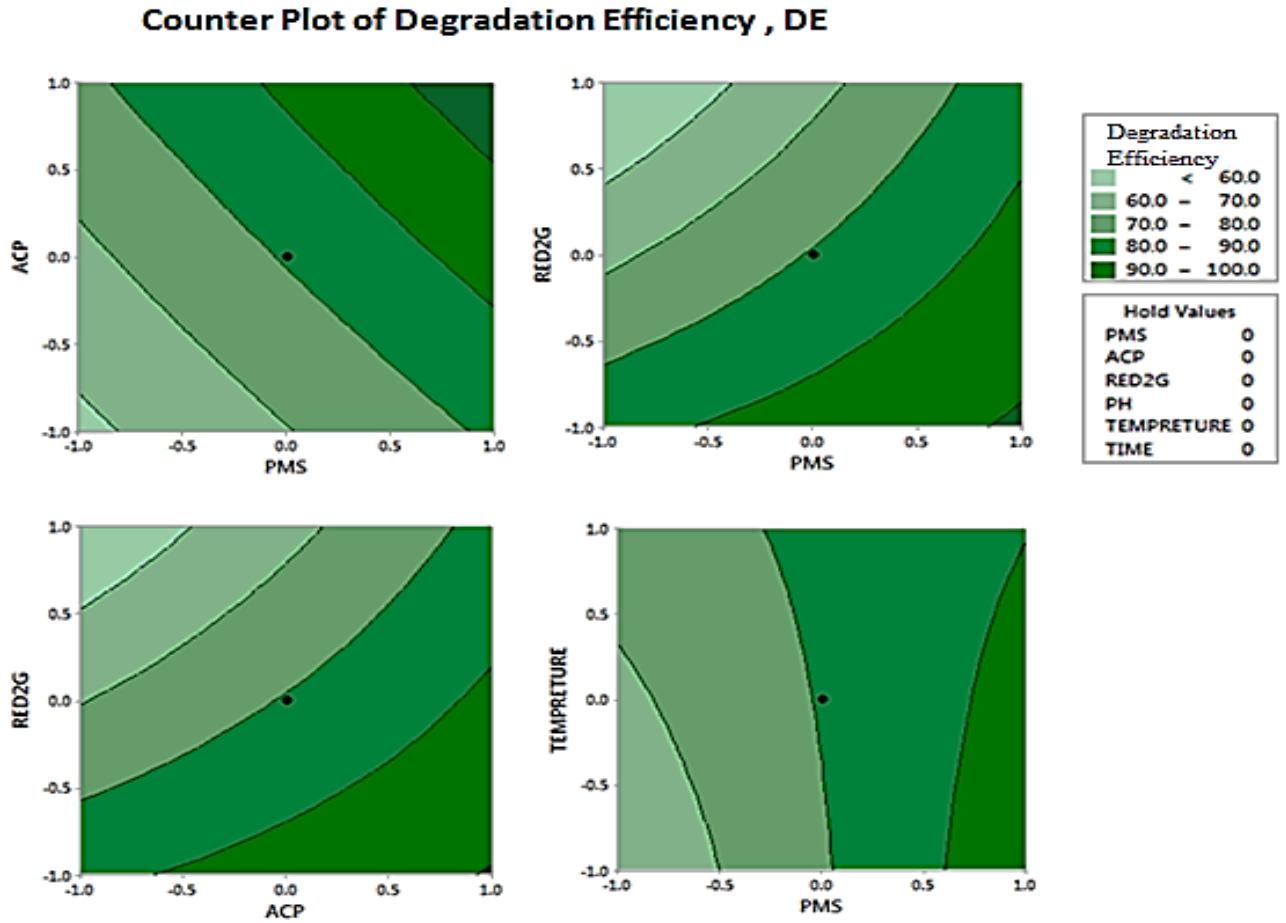

Fig 10: Response Contour Plots for the Degradation Efficiency,(DE%). Dark Green Regions Indicate that the Maximum DE Can be Achieved Using the Described Factorial Combination

shows a 2D plot for degradation efficiency with respect to the different two factorial combinations. As presented below, DE of 90-100% could be obtained at PMS concentration of 3mM and ACP dosage between 0.6-1.0 g/L. According to Table 6, the optimum conditions leading to the maximum response (i.e., the individual desirability function, d) were acquired by applying the Minitab response optimizer. On the basis of the individual response optimization, it is proved that a DE value of 100% can be obtained with a d = 1.0000 by utilizing a factorial blend of PMS=3.0 mM, ACP=1.0 g/L, pH=3.0 and time= 80 min at room temperature for Red-2G concentration of 60 mg/L.

In the final step, the following study was performed to evaluate the ability of the PMS/ACP-850 system in dye degradation process. According to the response function (Eq. (4)), the DE value of 100% can be achieved under the following conditions of PMS=6.0 mM, ACP=2.0 g/L, pH=3.0, temperature= 55 °C and time= 180 min for Red-2G concentration of 175 mg/L, being proved by the real experimental result obtained in the laboratory.

This result showed that the studied degrading system, which is based on carbon materials, has a high ability to decompose pollutants including azo dyes in high concentrations, which is in agreement with the literature [34].

Desorption Studies for Determination of the Contribution of Adsorption Phenomena in the Degradation Process

Basically, desorption studies facilitate the clarification of the mechanism and recovery of the adsorbate and activated carbon as a sorbent. Desorption tests (Fig. S2) indicated that the maximum dye releasing of 90.5% for Red-2G dye was obtained in aqueous solution at pH= 12. As observed, the initial pH of the water affects the dye amount desorbed from the ACP-850 surface. By increasing pH of the system, the number of positively charged sites is reduced, being suitable for the desorption process of Red-2G dye. Indeed, without dye desorption in water at pH= 2, the desorption efficiency was observed to be continuously enhanced until pH= 12, reaching a maximum value (90.5%). For strong acidic solutions (having considerably lower pH than pH_{PZC} of 7.1 determined for the ACP-850 sample used), the anionic dye adsorption is favored owing to enhanced electrostatic interaction occurring between positive charges induced on the ACP-850 surface [111] and the anionic dye, which is not suitable for dye desorption. Alternatively, for $pH>pH_{PZC}$ of 7.1, the generation of negative charges on the ACP-850 surface is favored due to the alkalinity, thereby increasing the anionic dye repulsion. In turn, this causes the desorption efficiency to be increased.

Finally, a test was performed under the optimum performance conditions, and the activated carbon used was separated and dried for the next step. The sorbent was then agitated with distilled water (200 mL) at pH of 12 during 24 h in order to complete the desorption process. In the following process, the desorbed dye was measured, and the result was 5.5 ppm. Accordingly, by considering the desorption efficiency (90.5% for 60 ppm), it can be stated that the contribution of adsorption in the red-2G dye removal process is 10.2%, indicating the importance of the catalytic role of the produced activated carbon (ACP-850) in the dye degradation process.

Reusability of ACP-850

The reuse experiment was carried out to detect the recovery performance of ACP-850 by the following procedure: ACP-850 was collected after each process, washed with ultrapure water, and dried at 105 °C for 2 h. All the actions were then accomplished under operation conditions the same as the previous runs. It is important to note that the slight weight loss of the catalyst in the fourth and fifth cycles is adjusted by dye concentration in the solution. In other words, the proportion of the catalyst weight to the dye concentration remains equal in all runs. Essentially, carbonaceous materials may lose their activation capacity following a period of use, arising from the surface deactivation. Probably, the decrease in the catalytic capability of ACP-850 can be attributed to the blockage of adsorption and catalytic active sites by intermediate products formed at the time of degradation process [112, 113]. As demonstrated in Fig. S3, reuse experiments indicate that the ACP-850 catalyst possesses suitable reusability with Red-2G efficiency after 5^{th} cycles under the following condition. When ACP-850 was used for the fifth time, the degradation efficiency of Red-2G was still over 65% in 1 h reaction time since the ACP with ultra-high surface area was present in the solution as PMS activator.

COD and TOC Removal

The analysis of total organic carbon (TOC) reflects the degree of mineralization of organic compounds, and the analysis of required chemical oxygen shows the degree of oxidation of organic compounds, indicating the progress of the color degradation reaction. The reduction of TOC level for Red-2G was 47.4% and 67.8% after 1.5 h and 24 h, respectively. It can be concluded that the complete degradation and semi-complete mineralization of the dye molecules occur after 1.5 h, which in turn indicate that almost half of the dye content is oxidized to carbon dioxide during the experiment. Consequently, the TOC removal rate is considerable and significant [114]. Likewise, the reduction of the COD level of red-2-G dye solution is equal to 70.8% and 84.3% after 1.5 and 24 h, respectively. The COD/TOC parameter (so-called the oxidation feasibility index) is reduced from 1.83 to 0.98 with the passage of time, indicating that the speed of the oxidation phenomenon is higher than the mineralization phenomenon at the beginning of the reaction. With the passage of time, this ratio decreases by the reduction of oxidizable species [3]. The results are well illustrated in Fig. S4.

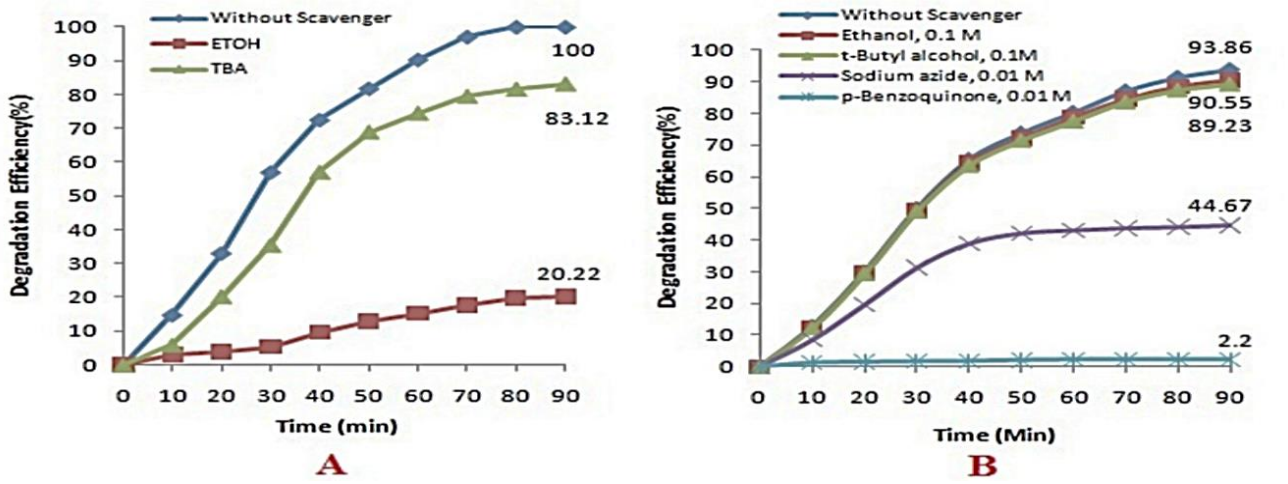

Fig 11: Effect of radical scavengers on R2G degradation efficiency at acidic (A) and basic (B) conditions; A) [Red-2G]=0.12 mM, [ACP]=1.0 g/L, [PMS]=3.0 mM, pH=3.0, and T=25 °C, B) [Red-2G]=0.12 mM, [ACP]=1.0 g/L, [PMS]=3.0 mM, pH=10.50, and T=25 °C

Influence of Waste Water Media on Degradation Efficiency of Red-2G

The degradation efficiency of the PMS activated system can be affected by waste water based on two main groups existing in the waste water media. The first one is the anions, inducing different effects on the hydroxyl and sulfate radicals created by the PMS activation. In fact, chloride ion is considered the main anion in different water samples. It has been proved that the chloride ion can increase the acetaminophen removal rate when the chloride concentration is higher than 20 mM in the sample [115]. Also, phosphate, nitrate, nitrite, carbonate, and bicarbonate ions have negative effects on the hydroxyl and sulfate radicals. The reason is that these ions can extinguish the aforementioned radicals [7]. The second one is organic matter, being a complex constituent in water media. Natural organic materials have been shown to play a negative role in the organic contaminant removal by activation of PMS [116]. According to Fig. S5, the monitoring of the Red-2G degradation in the actual wastewater is realized. Following the obtained results, Red-2G removal rate decreases compared to the control experiment. In the case of the control experiment, complete degradation (100%) is achieved after 80 min, whereas the degradation efficiency is 86.83 % and 95.8% after 80 and 90 min in the waste water experiment, respectively.

Characterization of Reactive Radicals

Radical quenching experiments were carried out using tertiary-butyl alcohol (TBA) and ethanol (EtOH) in acidic condition, allowing for the identification of the radical species produced in the PMS/ACP-850 process. For radical quenching experiments in basic condition, four reagent including TBA, EtOH, sodium azide (NaN_3) and p-benzoquinone were used [7]. In fact, the reaction between organic compound and radical species is challenging due to the presence of the alcohol, so that the degradation rate is expected to be reduced. An extremely prohibition occurrence took place when adding the EtOH to the degradation system as the α-hydrogen containing alcohol. Essentially, EtOH scavenges both of radicals ($SO_4^{-\bullet}$ and $^{\bullet}OH$) (($K_{ETOH-\bullet OH}$ =(1.8-2.8)×10^9 $M^{-1}S^{-1}$, $K_{ETOH-SO4-\bullet}$ =(1.6-7.7)×10^7 $M^{-1}S^{-1}$)), whereas TBA is the scavenger of $^{\bullet}OH$ since it does not contain α-hydrogen and possesses a considerably higher tendency to scavenge hydroxyl radical (($K_{TBA-\bullet OH}$ =(3.8-7.6)×10^8 $M^{-1}S^{-1}$, $K_{TBA-SO4-\bullet}$ =(4.0-9.1)×10^5 $M^{-1}S^{-1}$)). Based on Fig. 11-A, the presence of 0.1 M EtOH considerably suppresses the oxidation process, so that the decolorization efficiency is reduced from 100.0 to 20.2 % for Red-2G after 90 min. For TBA-added system, the presence of 0.1 M TBA leads to the suppression of the oxidation process, thereby decreasing decolorization efficiency from 100.0% to 83.1%.

Thus, the efficiency decrease rates of EtOH and TBA systems are found to be 79.8% and 16.9%, respectively. Alternatively, at acid condition, sulfate radicals are known as major active species, being a strong oxidant due to their high oxidation potential (2.5–3.1 V). These radicals are produced when the peroxo-bond of PMS is broken during the experiment. Furthermore, the half-life time of sulfate

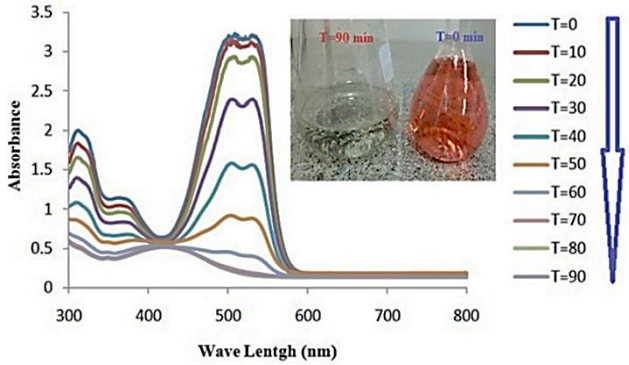

Fig 12: UV-Visible Spectra for the Degradation of Red-2G in ACP-850-PMS System: [Red-2G]$_o$= 0.12mM (60mg/l), [ACP-850]= 1.0 g/L, [PMS]= 3.0 mM, pH=3.0, and T= 25 °C

radicals is higher than that of hydroxyl radical (30–40 µs vs. 20 ns), owing to their reaction ability with organic species during the electron transfer. Nevertheless, hydroxyl radicals behave randomly, participating in different reactions with the same propensity [7].

Based on Fig. 11-B, the addition of tert-butyl alcohol (0.1 M) does not lead to the inhibition of the decolorization of Red-2G at basic condition (pH=10.5), indicating that hydroxyl radicals may not act as the reactive oxygen species. Similar results are acquired when ethanol (0.1 M; acting as the scavenger of both sulfate radical and hydroxyl radical) is added to the PMS/ACP-850 system, implying that hydroxyl and sulfate radicals are not the reactive oxygen species responsible for Red-2G degradation in the PMS/ACP-850 system at basic condition. Nevertheless, when sodium azide (0.01 M; a unique scavenger for $^1O2$ with a rate constant of 2×10^9 $M^{-1}S^{-1}$) is added to the reaction mixture, the decolorization of Red-2G is dramatically suppressed from 93.86% to 44.67%, demonstrating that sin $^1O2$ may be taken into account as one of the reactive oxygen species in this system at basic condition. Notwithstanding, $^1O2$ cannot be considered the only reactive species since the addition of sodium azide did not completely lead to the suppression of the Red-2G degradation. Additionally, when p-benzoquinone (0.01 M; a scavenger of superoxide anion radical with a rate constant of $0.9\text{-}1.0\times10^9$ $M^{-1}S^{-1}$) is added to the solution, degradation of Red-2G is completely inhibited as the degradation efficiency is reduced to 2.2%, indicating that superoxide anion radical is effective in the decolorization of Red-2G at basic condition. Finally, based on Fig. 11, both $SO_4^{\bullet-}$ and $^{\bullet}OH$ play roles in the process of degradation. Nevertheless, due to the remarkable difference between the efficiency decrease rates and the fact that sulfate radical is the primary reactive species at acid condition, $SO_4^{\bullet-}$ plays an essential role in PMS/ACP-850 system [7]. On the other hand, while singlet oxygen and superoxide anion radical are the reactive species in the basic condition, the latter plays a key role in the decolorization of Red-2G at pH=10.5 in the aforementioned system [109].

UV-Vis Spectra and Degradation Process

The dye solution color gradually decomposed as the reaction progressed in the PMS/ACP-850 system, being indicative of a decrease in the Red-2G concentration. Fig. 12 shows UV-Vis spectra recorded for the Red-2G during degradation process after 0, 10, 20, 30, 40, 50, 60, 70, 80, and 90 min. Basically, the Red-2G consists of an azo bond (N=N), a benzene ring and naphthalene ring, all of which leads to different absorbance peaks. The maximum value of absorption wavelength for Red-2G is 531 nm, producing the red color that can be ascribed to the azo bond.

Furthermore, the UV region shows three bands; the weakest one at 364 nm is related to the amide group connected to the naphthalene ring. The other band located at 312 nm is assigned to the naphthalene ring, and the most intense band is correlated with the benzene ring at 236 nm [117]. By proceeding the degradation reactions, the visible band remarkably decreases, which essentially arises from the fragmentation of the azo links by the oxidation process. Moreover, the decrease in the absorbance intensity at 236 and 312 nm evidences aromatic fragment degradation in the dye molecule as well as in its intermediates.

Proposed Mechanism for Degradation

According to the previous works, it is possible to identify the degradation intermediates generated in the PMS/ACP-850 system at different times on the basis of LC/MS technologies [3, 118]. To clarify the possible degradation mechanism at acidic and basic conditions, the molecular structure of possible intermediates is depicted in Schemes 1 and 2 for acidic condition, and in Scheme 3 for basic condition. The main peak of Red-2G is not observed after 90 min of reaction, demonstrating that the Red-2G is degraded totally. Other peaks are related to intermediate compounds in the Red-2G degradation process. The three main mechanisms involved in the first step of radical

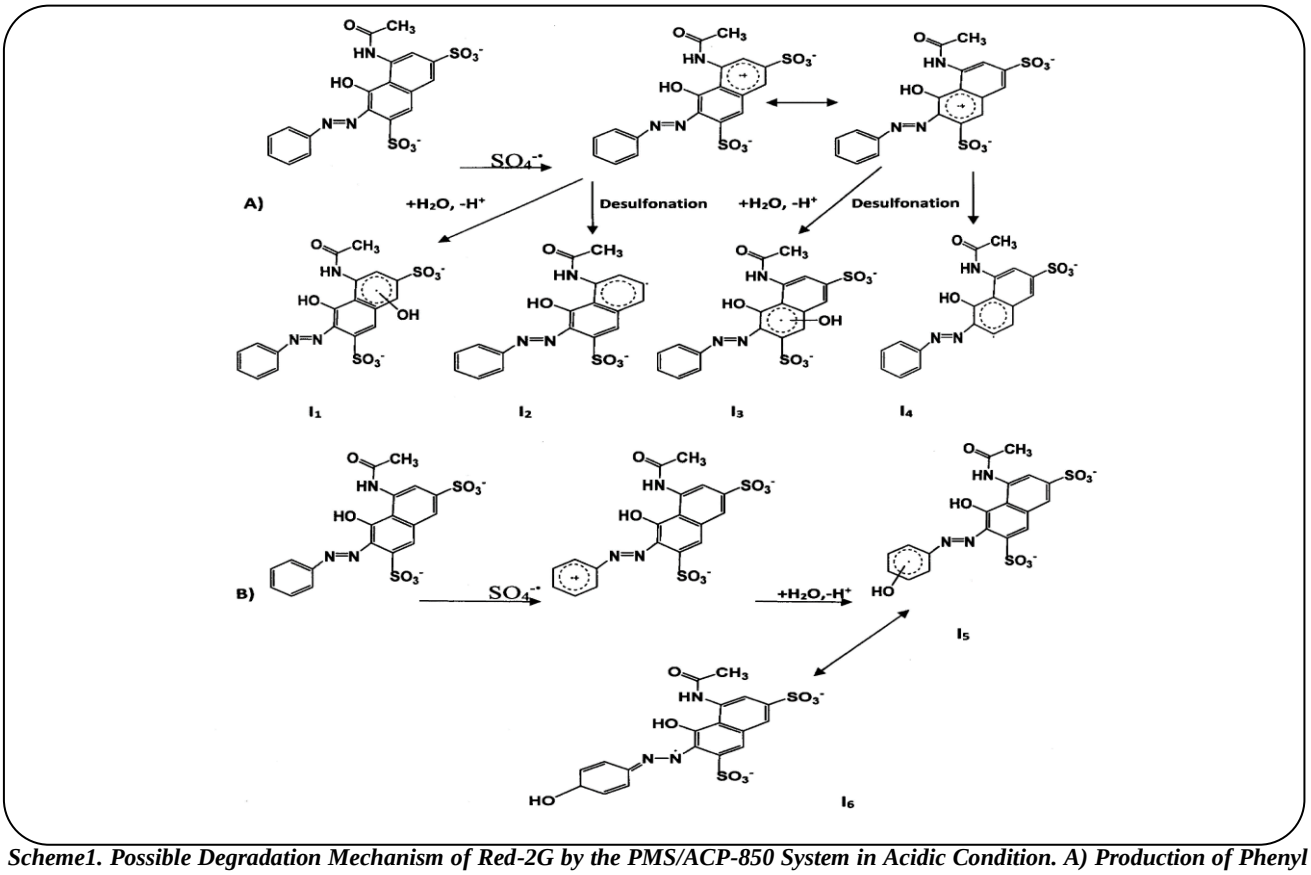

Scheme1. Possible Degradation Mechanism of Red-2G by the PMS/ACP-850 System in Acidic Condition. A) Production of Phenyl Radical Cation in the Naphthalene Part of Red-2G Molecule through SET Pathway, and B) Production of Phenyl Radical Cation in the Phenyl Azo Part, that is in the Resonance with AZO Bond

oxidation of aromatic compounds by $SO_4^{-\bullet}$ are as follows: radical adduct formation (RAF), hydrogen atom abstraction (HAA), and single electron transfer (SET) [119]. Note that the SET reaction is considered the fastest and simplest among all chemical reactions. Based on previous investigations, the overall reactivity of $SO_4^{-\bullet}$ has been shown to be significantly dependent on electron donating/withdrawing characteristics of functional groups existing in organic compounds [120]. However, for aromatic compounds containing both groups, it appears that the electron donating groups compete with the electron withdrawing groups for most aromatic compounds in the SET reactions. This occurrence is similar to the reactions induced by electrophilic aromatic substitution, whereby electron-withdrawing groups are controlled by electron-donating ones in ring activation and directing effects [119]. In the Red-2G molecule, hydroxyl (-OH), Azo (ph-N=N-) and amide (CH_3CONH-) substitutions act as electron donating groups, whereas the sulfur trioxide ($-SO_3^-$) plays the role of electron-withdrawing group for the aromatic ring. Based on the LC/MS/MS data of the present study and previous investigations, it has been shown that the SET pathway (as the main reaction mechanism) is responsible for the degradation of Red-2G from the aromatic ring. It also leads to the production of a phenyl radical cation, thereby reacting with water to add a hydroxyl group to the ring [119]. In this respect, Scheme 1 is proposed as the Red-2G degradation mechanism. As shown in Scheme 1, the mechanism is described in two separate sections (A and B), pertaining to the naphthalene and phenyl azo parts, respectively. The sulfate anion radical $SO_4^{-\bullet}$ may attack both rings of the naphthalene part and produce cation radical. In the following, each cation radical has two possibilities for progress. In the first path, it can react with water to generate hydroxyl cyclohexadienyl radicals (I_1,I_3). In the second path, it may lose sulfur trioxide to generate phenyl radical (I_2,I_4). Meanwhile, the sulfate anion radical $SO_4^{-\bullet}$ can attack the ring of phenyl azo part as indicated in section B of Scheme 1.

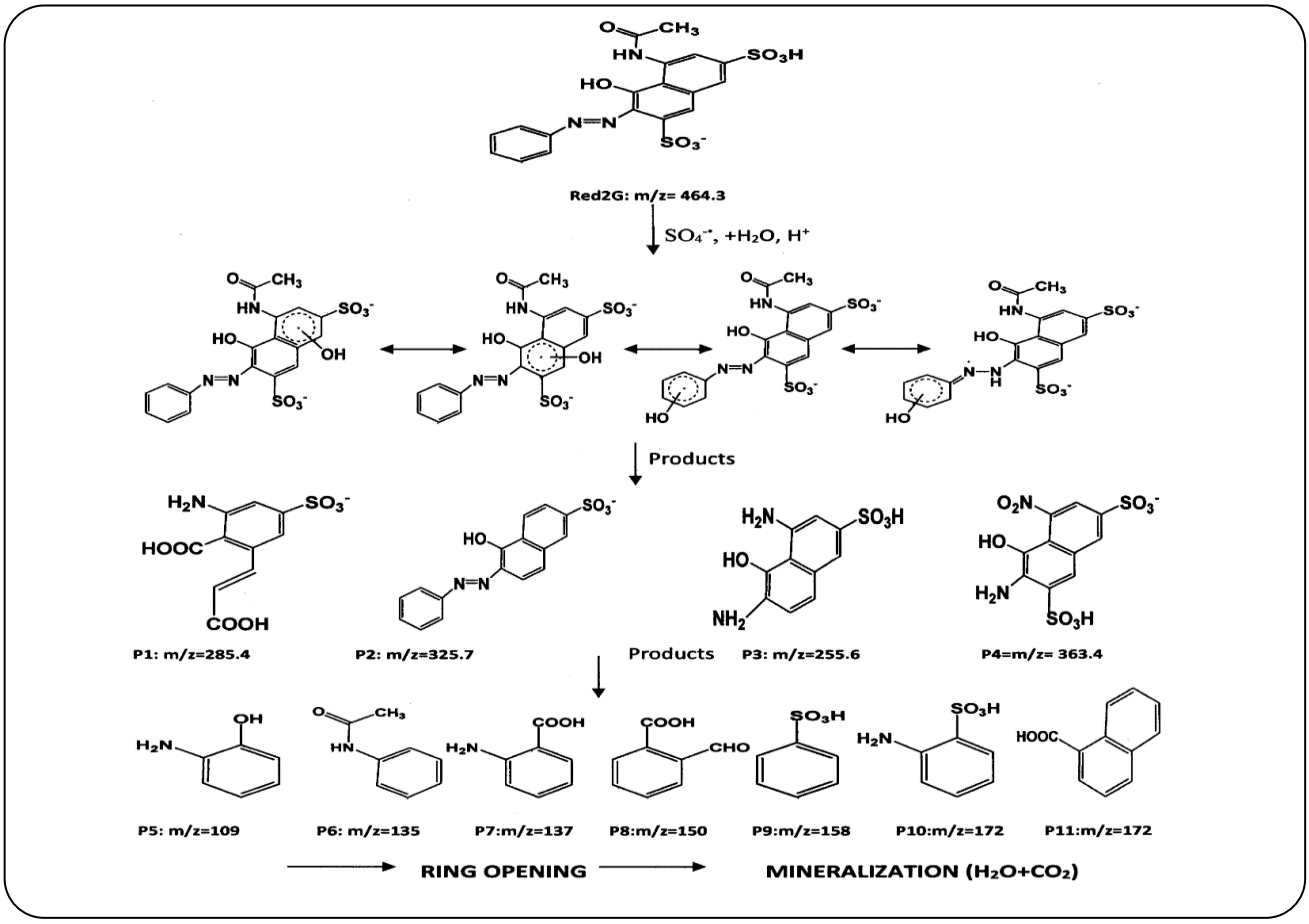

Scheme 2: Identified peaks in the LC/MS/MS diagram

The produced cation radical reacts with water to generate hydroxy cyclohexadienyl radical (I_5), which can be converted to the azo radical (I_6) via resonance with azo bond. The peaks with *m/z*= 285.4 (**P_1**), 325.7 (**P_2**), 255.6 (**P_3**), 363.4 (**P_4**), 109.0 (**P_5**), 135.0 (**P_6**), 137.0 (**P_7**), 150.0 (**P_8**), 158.0 (**P_9**), 172.0 (**P_{10}**), and 172.0(**P_{11}**) are identified (see Scheme 2). Fig. S6 presents TIC and MS spectra obtained from degradation products of fRed-2G. The detection of reaction intermediates in the LC/MS/MS diagram is difficult due to the short lifetime of radical cations (0.1-1 µs) generated in SET reactions [119]. The mineralization of the ring-opening products is the final step.

Based on the results obtained by LC/MS/MS analysis for basic condition, Scheme 3 illustrates a feasible pathway for Red-2G degradation in the PMS/ACP-850 system. The degradation process is assumed to be initiated by the separation of azo links because of the oxidative attack of $^1O_2$ or $O_2^{\bullet-}$, being generated from PMS by the activation in the basic condition [109]. The free radicals ($^1O_2$ or $O_2^{\bullet-}$) produce sulfanilic acid products that can easily dissolve in water. Therefore, they can be detected by the LC/MS/MS technique. Further oxidation and desulfurization lead to the generation of mostly aliphatic organics such as carboxylic acids, and the mineralization step occurs at the end of the process.

Performance Comparison of the Method

Based on Table 7, different performances occurred when using varied carbonaceous materials (especially activated carbon as catalysts) for the degradation of the organic compounds with known concentration. This confirmed that different catalytic performances in the degradation system can be obtained by various modified methods. In fact, differences in surface properties and pore structure of catalysts may influence the number of active sites, mass transfer of pollutants, oxidant molecules and dispersion of active components, thus directly affecting the degradation efficiency [121]. In the case of ACP-850 with high surface area (as confirmed by S_{BET} data), larger adsorption capacity and higher number of active sites as well as lower

Table 7: Carbon-Based Materials Activated by PMS for Degradation of Organic Contaminants

Pollutant	Pollutant concentration mg/L	PMS concentration mM	Carbon-based material ,g/L	Time (h)	Degradation (%)	Reference
Red-2G	175	6.0	ACP-850(1+2) ,2.0	3.0	100	This Study
MO , MB	25	3.0	ACP-800(1+2) ,0.5	1.5	100	[47]
Orange G	20	1.76	Activated carbon fiber, 0.3	0.83	100	[125]
Triclosan	10	0.8	Sludge-derived biochar,1.0	2	100	[126]
Phenol	25	6.5	Powder Activated Carbon,0.2	0.25	100	[127]
AO7	20	3.2	Granular Activated Carbon,1.0	5.0	85	[128]
Rhodamin B	10	0.5	Biochar, 0.5	-	81.9	[129]
MB	50	0.3	N-doped Carbon, 0.3	-	98.7	[130]

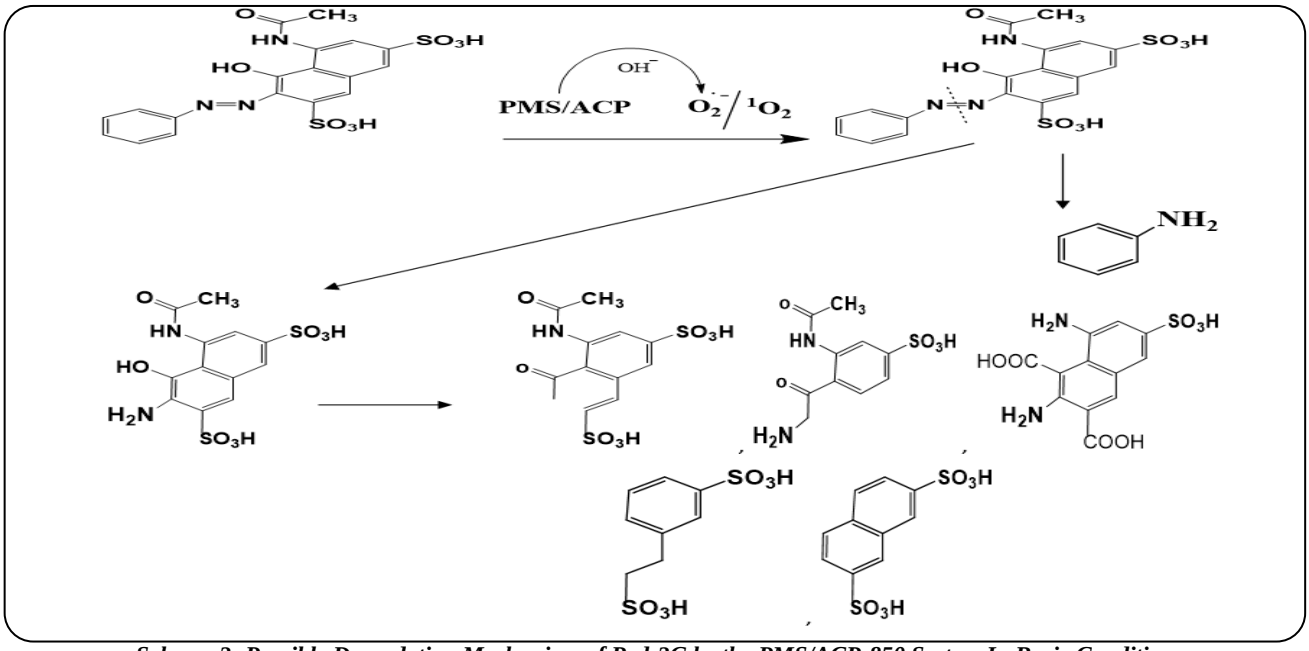

Scheme 3: Possible Degradation Mechanism of Red-2G by the PMS/ACP-850 System In Basic Condition

mass transfer resistance are expected to occur, being advantageous for ACP-850 to activate PMS as an oxidation agent. In addition, the increase in the Red-2G and PMS adsorption on the surface of the catalyst can facilitate the degradation in the electron transfer way [122, 123]. Consequently, the carbon configuration and porosity are considered two key factors for biomass-based activated carbon in advanced oxidation processes [124].

CONCLUSIONS

PNS-derived activated carbon has been proposed as a modified catalyst (ACP-850) with ultra-high surface area for activating PMS as a native activator to degrade Red-2G in water and waste water media. The key findings of this study are summarized as follows:

- The use of pistachio nutshell (PNS) for producing ACP-850, which is easily and affordably available in large quantities in Iran.
- The production of high surface area activated carbon (2318 m^2/g) by thermal treatment of the powdered biochar sample with potassium oxalate in the inert atmosphere as a green catalyst.
- The use of an intelligent approach (DSD) as a new design for simultaneous screening and optimization of the six variables at 3 levels by just 26 test runs.
- According to the response function, DE value of 100% could be achieved under the following conditions: PMS=6.0 mM, ACP=2.0 g/L, pH=3.0 and time= 180 min at room temperature for the Red-2G concentration of 170 mg/L. This concentration was the highest amount that was

degraded with PMS activation by agricultural waste-derived activated carbon compared to the previous studies.
- Based on the investigation performed on reusability, the possibility of the frequent use of ACP-850 in the dye degradation from the contaminated solution was confirmed.
- The radical quenching experiments showed that sulfate anion radical ($SO_4^{-\bullet}$) and superoxide anion radical ($O_2^{\bullet -}$) played key roles as reactive species in the PMS/ACP-850 system at acidic and basic conditions, respectively.
- As the main reaction mechanism, the SET pathway was found to be responsible for the degradation of Red-2G in acidic condition. Moreover, the degradation process was initiated by the separation of azo links, arising from the oxidative attack of $^1O_2$ or $O_2^{\bullet -}$ in the basic condition.

Acknowledgments

The authors express their appreciation to the university of Kashan for the financial support of this work under Grant number 463609.

Received : May.16, 2023 ; Accepted : Oct.02, 2023

REFERENCES

[1] Yadav A., Patel R.V., Labhasetwar P.K., Shahi V.K., Novel MIL101(Fe) Impregnated Poly(vinylidene Fluoride-co-Hexafluoropropylene) Mixed Matrix Membranes for Dye Removal from Textile Industryp Wastewater, *Journal of Water Process Engineering*, **43**: 102317 (2021).

[2] Dutta A.K., Ghorai U.K., Chattopadhyay K.K., Banerjee D., Removal of Textile Dyes by Carbon Nanotubes: A Comparison between Adsorption and UV Assisted Photocatalysis, *Physica E: Low-dimensional Systems and Nanostructures*, **99**: 6-15 (2018).

[3] Thomas S., Sreekanth R., Sijumon V.A., Aravind U.K., Oxidative Degradation of Acid Red 1 in Aqueous Medium, *Chemical Engineering Journal*, **244**: 473-482 (2014).

[4] de Aragao Umbuzeiro G., Freeman H.S., Warren S.H., De Oliveira D.P., Terao Y., Watanabe T., Claxton L.D., The Contribution of Azo Dyes to the Mutagenic Activity of the Cristais River, *Chemosphere*, **60(1)**: 55-64 (2005).

[5] Pinheiro H.M., Touraud E., Thomas O., Aromatic Amines from Azo Dye Reduction: Status Review with Emphasis on Direct UV Spectrophotometric Detection in Textile Industry Wastewaters, *Dyes and Pigments*,. **61(2)**: 121-139 (2004).

[6] Hou L., Li X., Yang Q., Chen F., Wang S., Ma Y., Wu Y., Zhu X., Huang X., Wang D., Heterogeneous Activation of Peroxymonosulfate Using Mn-Fe Layered Double Hydroxide: Performance and Mechanism for Organic Pollutant Degradation, *Science of The Total Environment*, **663**: 453-464 (2019).

[7] Ghanbari F., Moradi M., Application of Peroxymonosulfate and its Activation Methods for Degradation of Environmental Organic Pollutants: Review, *Chemical Engineering Journal*, **310**: 41-62 (2017).

[8] Yin R., Guo W., Wang H., Du J., Zhou X., Wu Q., Zheng H., Chang J., Ren N., Enhanced Peroxymonosulfate Activation For Sulfamethazine Degradation By Ultrasound Irradiation: Performances And Mechanisms, *Chemical Engineering Journal*, **335**: 145-153 (2018).

[9] Wang G., Nie X., Ji X., Quan X., Chen S., Wang H., Yu H., Guo X., Enhanced Heterogeneous Activation of Peroxymonosulfate by Co and N Codoped Porous Carbon for Degradation of Organic Pollutants: The Synergism between Co and N, *Environmental Science: Nano*, **6(2)**: 399-410 (2019)

[10] Xia X., Zhu F., Li J., Yang H., Wei L., Li Q., Jiang J., Zhang G., Zhao Q., A Review Study on Sulfate-Radical-Based Advanced Oxidation Processes for Domestic/Industrial Wastewater Treatment: Degradation, Efficiency, and Mechanism, *Front Chem*,. **8**: 592056 (2020).

[11] Arshadi M., Abdolmaleki M.K., Mousavinia F., Khalafi-Nezhad A., Firouzabadi H., Gil A., Degradation of Methyl Orange by Heterogeneous Fenton-Like Oxidation on a Nano-Organometallic Compound in the Presence of Multi-Walled Carbon Nanotubes, *Chemical Engineering Research and Design*, **112**: 113-121 (2016).

[12] Wang J., Chu L., Irradiation Treatment of Pharmaceutical and Personal Care Products (PPCPs) in Water and Wastewater: An Overview, *Radiation Physics and Chemistry*, **125**: 56 (2016).

[13] Miklos D.B., Remy C., Jekel M., Linden K.G., Drewes J.E., Hübner U., Evaluation of Advanced Oxidation Processes For Water And Wastewater Treatment – A Critical Review, *Water Research*, **139**: 118-131 (2018).

[14] Li S., Lin Q., Liu X., Yang L., Ding J., Dong F., Li Y., Irfan M., Zhang P., Fast Photocatalytic Degradation of Dyes Using Low-Power Laser-Fabricated Cu_2 O–Cu Nanocomposites, *RSC Advances*, **8**: 20277-20286 (2018).

[15] Tao X., Yang C., Huang L., Shang S., Novel Plasma Assisted Preparation of ZnCuFeCr Layered Double Hydroxides with Improved Photocatalytic Performance of Methyl Orange Degradation, *Applied Surface Science*, **507**: 145053 (2020).

[16] Umamaheswari C., Lakshmanan A., Nagarajan N.S., Green Synthesis, Characterization and Catalytic Degradation Studies of Gold Nanoparticles Against Congo Red and Methyl Orange, *J Photochem Photobiol B*, **178**: 33-39 (2018).

[17] Wen D., Li W., Lv J., Qiang Z., Li M., Methylene blue Degradation by the VUV/UV/Persulfate Process: Effect of pH on the Roles of Photolysis and Oxidation, **391**: 121855 (2020).

[18] Abbasi S., Magnetic Photocatalysts Based on Graphene Oxide: Synthesis, Characterization, Application in Advanced Oxidation Processes and Response Surface Analysis, *Applied Water Science*, **13(6)**: 128 (2023).

[19] Lai C., Wang M.M., Zeng G.M., Liu Y.G., Huang D.L., Zhang C., Wang R.Z., Xu P., Cheng M., Huang C., Wu H.P., Synthesis of Surface Molecular Imprinted TiO2/Graphene Photocatalyst and its Highly Efficient Photocatalytic Degradation of Target Pollutant under Visible Light Irradiation, *Applied Surface Science*, **390**: 368-376 (2016).

[20] Abbasi S., Dastan D., Ţălu Ş., Tahir M.B., Elias M., Tao L., Li Z., Evaluation of the Dependence of Methyl Orange Organic Pollutant Removal Rate on the Amount of Titanium Dioxide Nanoparticles in MWCNTs-TiO2 Photocatalyst Using Statistical Methods and Duncan's Multiple Range Test, *International Journal of Environmental Analytical Chemistry*, 1-15 (2022).

[21] Abbasi S., Studying the Destruction of Pollutant in the Presence of Photocatalysts Based on MWCNTs with Controlled Values of TiO2 Nanoparticles, *Applied Water Science*, **13(4)**: 100 (2023).

[22] Abbasi S., Hasanpour M., Ahmadpoor F., Sillanpää M., Dastan D., Achour A., Application of the Statistical Analysis Methodology for Photodegradation of Methyl Orange Using a New Nanocomposite Containing Modified TiO_2 Semiconductor with SnO_2, *International Journal of Environmental Analytical Chemistry*, **101**: 1-17 (2019).

[23] Abbasi S., Investigation of the Enhancement and Optimization of the Photocatalytic Activity of Modified TiO_2 Nanoparticles with SnO_2 Nanoparticles Using Statistical Method, *Materials Research Express*, **5** (2018).

[24] roozban N., Abbasi S., Ghazizadeh M., Statistical Analysis of the Photocatalytic Activity of Decorated Multi-Walled Carbon Nanotubes with ZnO Nanoparticles, *Journal of Materials Science Materials in Electronics*, **28** (2017).

[25] Abbasi S., Ekrami-Kakhki M.-S., Tahari M., The Influence of ZnO Nanoparticles Amount on the Optimisation of Photo Degradation of Methyl Orange Using Decorated MWCNTs, *Progress in Industrial Ecology, An International Journal*, **13**: 3 (2019).

[26] Heidari H., Aliramezani F., Ni /Fe3O4@ nanocellulose and Ni/Nanocellulose Green Nanocomposites: Inorganic- Organic Hybrid Catalysts for the Reduction of Organic Pollutants, *Iranian Journal of Chemistry and Chemical Engineering*, **41(10)**: (2022).

[27] Khuntia S., Majumder S., Ghosh P., Catalytic Ozonation of Dye in a Microbubble System: Hydroxyl Radical Contribution and Effect of Salt, *Journal of environmental chemical engineering*, **4**: 2250-2258 (2016).

[28] Muniyasamy A., Sivaporul G., Gopinath A., Lakshmanan R., Altaee A., Achary A., Chellam P.V., Process Development for the Degradation of Textile Azo Dyes (mono-, di-, poly-) by Advanced Oxidation Process - Ozonation: Experimental & Partial Derivative Modelling Approach, *Journal of Environmental Management*, **265**: 110397 (2020).

[29] Jamil A., Bokhari T.H., Iqbal M, Bhatti I.A., Zuber M., Nisar J., Masood N., Gamma Radiation and Hydrogen Peroxide Based Advanced Oxidation Process for the Degradation of Disperse Dye in Aqueous Medium, *Zeitschrift für Physikalische Chemie*, **234(2)**: 279-294 (2020).

[30] Arshad R., Bokhari T.H., Khosa K.K., Bhatti I.A., Munir M., Iqbal M., Iqbal D.N., Khan M.I., Iqbal M., Nazir A., Gamma Radiation Induced Degradation of Anthraquinone Reactive Blue-19 Dye Using Hydrogen Peroxide as Oxidizing Agent, *Radiation Physics and Chemistry*, **168**: 108637 (2020).

[31] Asgari G., Seid-mohammadi A., Rahmani A., Samadi M.T., Alizadeh S., Nematollahi D., Salari M., Carbon Felt Modified with N-doped rGO for an Efficient Electro-Peroxone Process in Diuron Degradation and Biodegradability Improvement of Wastewater from a Pesticide Manufacture: Optimization of Process Parameters, Electrical Energy Consumption and Degradation Pathway, *Separation and Purification Technology*, **274**: 118962 (2021).

[32] Asgari G., Seid-Mohammadi A., Rahmani A., Samadi M.T., Salari M., Alizadeh S., Nematollahi D., Diuron Degradation Using Three-Dimensional Electro-Peroxone (3D/E-Peroxone) Process in the Presence of TiO_2/GAC: Application for Real Wastewater and Optimization Using RSM-CCD and ANN-GA Approaches, *Chemosphere*, **266**: 129179 (2021).

[33] Rahmani A., Seid-Mohammadi A., Leili M., Shabanloo A., Ansari A., Electrocatalytic Degradation of Diuron Herbicide Using Three-Dimensional Carbon Felt/β-PbO2 Anode as a Highly Porous Electrode: Influencing Factors and Degradation Mechanisms, *Chemosphere*, **276**: 130141 (2021).

[34] Wang J., Wang S., Activation of Persulfate (PS) and Peroxymonosulfate (PMS) and Application for the Degradation of Emerging Contaminants, *Chemical Engineering Journal*, **334**: 1502-1517 (2018).

[35] Ma J., Ding Y., Chi L., Yang X., Zhong Y., Wang Z., Shi Q., Degradation of Benzotriazole by Sulfate Radical-Based Advanced Oxidation Process, *Environ Technol*,. **42(2)**: 238-247 (2021).

[36] Peng Y., Tang H., Yao B., Gao X., Yang X., Zhou Y., Activation of Peroxymonosulfate (PMS) by Spinel Ferrite and their Composites in Degradation of Organic Pollutants: A Review, *Chemical Engineering Journal*, **414**: 128800 (2021).

[37] Hussain S., Aneggi E., Goi D., Catalytic Activity of Metals in Heterogeneous Fenton-Like Oxidation of Wastewater Contaminants: A Review, *Environmental Chemistry Letters*, **19(3)**: 2405-2424 (2021).

[38] Kgatle M., Sikhwivhilu K., Ndlovu G., Moloto N., Degradation Kinetics of Methyl Orange Dye in Water Using Trimetallic Fe/Cu/Ag Nanoparticles, *Catalysts*,. **11(4)**: 428.

[39] Maleki A., Seifi M., Marzban N., Evaluation of Sonocatalytic and Photocatalytic Processes Efficiency for Degradation of Humic Compounds Using Synthesized Transition-Metal-Doped ZnO Nanoparticles in Aqueous Solution, *Journal of Chemistry*, **2021**: 9938579 (2021).

[40] Le V.T., Nguyen V.C., Cao X.T., Chau T.P., Nguyen T.D., Nguyen T.L., Doan V.D., Highly Effective Degradation of Nitrophenols by Biometal Nanoparticles Synthesized using Caulis Spatholobi Extract, *Journal of Nanomaterials*, **2021**: 6696995 (2021).

[41] Shahi N.K., Maeng M., Choi I., Dockko S., Degradation Effect of Ultraviolet-Induced Advanced Oxidation of Chlorine, Chlorine Dioxide, and Hydrogen Peroxide and its Impact on Coagulation of Extracellular Organic Matter Produced by Microcystis Aeruginosa, *Chemosphere*, **281**:130765 (2021).

[42] Huang Y., Kong M., Coffin S., Cochran K.H., Westerman D.C., Schlenk D., Richardson S.D., Lei L., Dionysiou D.D., Degradation of Contaminants of Emerging Concern by UV/H(2)O(2) for Water Reuse: Kinetics, Mechanisms, and Cytotoxicity Analysis, *Water Res*, **174**: 115587 (2020).

[43] Shariatzadeh S.M., Salimi M., Fathinejad H., Hassani Joshaghani A., Synthesis, Characterization, and Photocatalytic Application of α-Fe2O3/α-AgVO3 Nanocomposite for Removal of Methylene Blue from Aqueous Media, I*ranian Journal of Chemistry and Chemical Engineering*, **42(4)** (2022).

[44] Wang H., Xie R., Zhang J., Zhao J., Preparation and Characterization of Distillers' Grain Based Activated Carbon as Low Cost Methylene Blue Adsorbent: Mass Transfer and Equilibrium Modeling, *Advanced Powder Technology*, **29**: 27-35 (2018).

[45] Danish M., Ahmad T., Hashim R., Said N., Akhtar M.N., Mohamad-Saleh J., Sulaiman O., Comparison of Surface Properties of Wood Biomass Activated Carbons and their Application Against Rhodamine B and Methylene Blue Dye, *Surfaces and Interfaces*, **11** (2018).

[46] Al-Saghir M.G., Porter D.M., Taxonomic Revision of the Genus Pistacia L. (Anacardiaceae), *American Journal of Plant Sciences*, **2012**: 12-32 (2012).

[47]Gholami A., Mousavinia F., Eco-friendly Approach for Efficient Catalytic Degradation of Organic Dyes through Peroxymonosulfate Activated with Pistachio Shell-Derived Biochar and Activated Carbon, *Environmental Technology*, 1-18 (2021).

[48] Hamed M., Bougatef H., Karoud W., Krichen F., Haddar A., Bougatef A., Sila A., Polysaccharides Extracted from Pistachio External hull: Characterization, Antioxidant Activity and Potential Application on Meat as Preservative, *Industrial Crops and Products*, **148**:112315 (2020).

[49] Sevilla M., Ferrero G.A., Fuertes A.B., Beyond KOH Activation for The Synthesis of Superactivated Carbons from Hydrochar, *Carbon*, **114**: 50-58 (2017).

[50] Lee J.H., Park S.J., Potassium Oxalate as an Alternative Activating Reagent of Corn Starch-Derived Porous Carbons for Methane Storage, *J Nanosci Nanotechnol*, **20(11)**: 7124-7129 (2020).

[51] Cong Jing C.J., Wen Gang W.G., Huang TingLin H.T., Deng LinYu D.L., Ma Jun M.J., Study on Enhanced Ozonation Degradation of Para-Chlorobenzoic Acid by Peroxymonosulfate in Aqueous Solution, *Chemical Engineering Journal*, **264**: 399-403 (2015).

[52] Hu P., Long M., Cobalt-catalyzed Sulfate Radical-Based Advanced Oxidation: A Review on Heterogeneous Catalysts and Applications, *Applied Catalysis B: Environmental*, **181**: 103-117 (2016).

[53] Ferreira S.L., Bruns R.E., da Silva E.G., Dos Santos W.N., Quintella C.M., David J.M., de Andrade J.B., Breitkreitz M.C., Jardim I.C, Neto B.B., Statistical Designs and Response Surface Techniques for the Optimization of Chromatographic Systems, *Journal of Chromatography A*, **1158(1)**: 2-14 (2007).

[54] Georgiou S.D., Stylianou S., Aggarwal M., Efficient three-Level Screening Designs Using Weighing Matrices, *Statistics*, **48(4)**: 815-833 (2014).

[55] Priyadharshini S.D., Bakthavatsalam A., Optimization of Phenol Degradation by the Microalga Chlorella Pyrenoidosa Using Plackett–Burman Design and Response Surface Methodology, *Bioresource technology*, **207**: 150-156 (2016).

[56] Jones B., Nachtsheim C.J., A Class of Three-Level Designs for Definitive Screening in the Presence of Second-Order Effects, *Journal of Quality Technology*, **43(1)**: 1-15 (2011).

[57] Tang D., Zhang G., Guo S., Efficient Activation of Peroxymonosulfate by Manganese Oxide for the Degradation of Azo Dye at Ambient Condition, *Journal of Colloid and Interface Science*, **454**: 44-51 (2015).

[58] Shoniya Thomas S.T., Abraham S.V., Aravind U.K., Aravindakumar C.T., Enhanced Degradation of Acid Red 1 Dye Using a Coupled System of Zero Valent Iron Nanoparticles and Sonolysis, *Environmental Science and Pollution Research*, **24(31)**: 24533-24544 (2017).

[59] Kumari L., Tiwary D., Mishra P.K., Biodegradation of C.I. Acid Red 1 by indigenous Bacteria Stenotrophomonas sp. BHUSSp X2 Isolated from Dye Contaminated Soil, *Environmental Science and Pollution Research*, **23(5)**: 4054-4062 (2016).

[60] Deniz F., Kepekçi R.A., Dye Biosorption onto Pistachio By-Product: A Green Environmental Engineering Approach, *Journal of Molecular Liquids*, **219**: 194-200 (2016).

[61] Moussavi G., Barikbin B., Biosorption of Chromium(VI) from Industrial Wastewater onto Pistachio Hull Waste Biomass, *Chemical Engineering Journal*, **162**: 893-900 (2010).

[62] Gong J.L., Wang B., Zeng G.M., Yang C.P., Niu C.G., Niu Q.Y., Zhou W.J., Liang Y., Removal of Cationic Dyes from Aqueous Solution Using Magnetic Multi-Wall Carbon Nanotube Nanocomposite as Adsorbent, *J Hazard Mater*, **164(2-3)**: 1517-22 (2009).

[63] Çelebi H., Gök G., Gök O., Adsorption Capability of Brewed Tea Waste in Waters Containing Toxic lead(II), Cadmium (II), Nickel (II), and zinc(II) Heavy Metal Ions, *Scientific Reports*, **10(1)**: 17570 (2020).

[64] Foo K.Y., Hameed B.H., Preparation and Characterization of Activated Carbon from Pistachio Nut Shells via Microwave-Induced Chemical Activation, *Biomass and Bioenergy*, **35(7)**: 3257-3261 (2011).

[65] El-Shafie A.S., Khashan A.W., Hussein Y.H., El-Azazy M., Application of a Definitive Screening Design for the Synthesis of a Charge-Transfer Complex of Sparfloxacin with Tetracyanoethylene: Spectroscopic, Thermodynamic, Kinetics, and DFT Computational Studies, *RSC Advances*, **9(43)**: 24722-24732.

[66] Anipsitakis G.P. D.D., Dionysiou, Degradation of Organic Contaminants in Water with Sulfate Radicals Generated by the Conjunction of Peroxymonosulfate with Cobalt, *Environ. Sci. Technol.*, **37(20)**: 4790-7 (2003).

[67]Anipsitakis G.P., Cobalt/Peroxymonosulfate And Related Oxidizing Reagents For Water Treatment, (2005).

[68] Wacławek S., Grübel K., Černík M., Simple Spectrophotometric Determination of Monopersulfate, *Spectrochim Acta A Mol Biomol Spectrosc*, **149**: 928-33 (2015).

[69] Hussain H., Green I.R., Ahmed I., Journey Describing Applications of Oxone in Synthetic Chemistry, *Chemical Reviews*, **113(5)**: 3329-3371 (2013).

[70] Pang X., Guo Y., Zhang Y., Xu B., Qi F., LaCoO3 Perovskite Oxide Activation of Peroxymonosulfate for Aqueous 2-Phenyl-5-Sulfobenzimidazole Degradation: Effect of Synthetic Method and the Reaction Mechanism,*Chemical Engineering Journal*, **304** (2016).

[71] Pang X., Guo Y., Zhang Y., Xu B., Qi F., LaCoO3 Perovskite Oxide Activation of Peroxymonosulfate for Aqueous 2-Phenyl-5-Sulfobenzimidazole Degradation: Effect of Synthetic Method and the Reaction Mechanism, *Chemical Engineering Journal*, **304**: 897-907 (2016).

[72] Douara N., Benzekri Benallou M., Termoul M., Mekibes Z., Bestani B., Removal of Textile Dyes on a Biosorbent Based on the Leaves of Atriplex Halimus, *Iranian Journal of Chemistry and Chemical Engineering*, (2023).

[73] Abbasi S., Response Surface Methodology for Photo Degradation of Methyl Orange Using Magnetic Nanocomposites Containing Zinc Oxide, *Journal of Cluster Science*, **32** (2021).

[74] Roozban N., Abbasi S., Ghazizadeh M., The Experimental and Statistical Investigation of the Photo Degradation of Methyl Orange Using Modified MWCNTs with Different Amount of ZnO Nanoparticles, *Journal of Materials Science: Materials in Electronics*, **28**:7343-52 (2017).

[75] Younes A., Ali J.S., Nur M.T., Duda A., Wang J., Samson J., Kawamura A., Francesconi L., Alexandratos S., Drain C.M., Pistachio Shells as Remediating Agents for Uranium in Contaminated Industrial Seawater, *J Environ Radioact*, **217**: 106209 (2020).

[76] Yang H., Yan R., Chen H., Lee D.H., Zheng C., Characteristics of Hemicellulose, Cellulose and Lignin Pyrolysis, *Fuel*, **86(12)**: 1781-1788 (2007).

[77] Baytar O., Ceyhan A.A., Şahin Ö., Production of Activated Carbon from Elaeagnus Angustifolia Seeds Using H(3)PO(4) Activator and Methylene Blue and Malachite Green Adsorption. Int J Phytoremediation, **23**(7): 693-703 (2021).

[78] Oliveira M., Treatment of Effluents Containing 2-Chlorophenol by Adsorption Onto Chemically and Physically Activated Biochars, *Journal of Environmental Chemical Engineering*, **8(6)**: 104473 (2020).

[79] Cui H., Xu J., Shi J., You S., Zhang C., Yan N., Liu Y., Chen G., Evaluation of Different Potassium Salts as Activators for Hierarchically Porous Carbons and their Applications in CO2 Adsorption, *Journal of colloid and interface science*, **583**: p. 40-49 (2020).

[80] Mansour F., Al-Hindi M., Yahfoufi R., Ayoub G.M., Ahmad M.N., The Use of Activated Carbon for the Removal of Pharmaceuticals from Aqueous Solutions: A Review, *Reviews in Environmental Science and Bio/Technology*, **17** (2018).

[81] Vunain E., Biswick T., Adsorptive Removal of Methylene Blue from Aqueous Solution on Activated Carbon Prepared from Malawian Baobab Fruit Shell Wastes: Equilibrium, Kinetics and Thermodynamic Studies, *Separation Science and Technology*, **54(1)**: 27-41 (2019).

[82] Konsolakis M., Assessment of Biochar as Feedstock in a Direct Carbon Solid Oxide Fuel Cell, *RSC Advances*, **5(90)**: 73399-409 (2015).

[83] Pongener C.H., Kibami D.A., Rao K.S., Goswamee R.L., Sinha D., Synthesis and Characterization of Activated Carbon from the Biowaste of the Plant Manihot Esculenta, **4(1)**: 59-68 (2015).

[84] Njewa J.B., Vunain E., Biswick T., Synthesis and Characterization of Activated Carbons Prepared from Agro-Wastes by Chemical Activation, *Journal of Chemistry*, **2022**: 9975444 (2022).

[85] Yaman S., Pyrolysis of Biomass to Produce Fuels and Chemical Feedstocks, *Energy Conversion and Management*, **45(5)**: 651-671 (2004).

[86] Liu Z., Quek A., Hoekman S.K., Balasubramanian R., Production of Solid Biochar Fuel from Waste Biomass by Hydrothermal Carbonization, *Fuel*,. **103**: 943-949 (2013).

[87] Cao X., Harris W., Properties of Dairy-Manure-Derived Biochar Pertinent to its Potential Use in Remediation, *Bioresour Technol*, **101(14)**: 5222-8 (2010).

[88] Sharma R.K., Wooten J.B., Baliga V.L., Lin X., Chan W.G., Hajaligol M.R., Characterization of Chars from Pyrolysis of Lignin, *Fuel*, **83**: 1469 (2004).

[89] Komnitsas K., Zaharaki D., Pyliotis I., Vamvuka D., Bartzas G., Assessment of Pistachio Shell Biochar Quality and Its Potential for Adsorption of Heavy Metals, *Waste and Biomass Valorization*, **6(5)**: 805-816 (2015).

[90] Ma X., Yang H., Yu L., Chen Y., Li Y., Preparation, Surface and Pore Structure of High Surface Area Activated Carbon Fibers from Bamboo by Steam Activation, *Materials (Basel)*, **7(6)**: 4431-4441 (2014).

[91] Jones B., Nachtsheim C.J., Definitive Screening Designs with Added Two-Level Categorical Factors, *Journal of Quality Technology*, **45(2)**: 121-129 (2013).

[92] El-Azazy M., El-Shafie A.S., Ashraf A., Issa A.A., Eco-Structured Biosorptive Removal of Basic Fuchsin Using Pistachio Nutshells: A Definitive Screening Design—Based Approach, *Applied Sciences*,. **9(22)**: 4855 (2019).

[93] Elsayed M.S., Eldadamony N.M., Alrdahe S.S., Saber WI., Definitive Screening Design and Artificial Neural Network for Modeling a Rapid Biodegradation of Date Palm Fronds by a New Trichoderma sp. PWN6 into Citric Acid, *Molecules*, **26(16)**: 5048 (2021).

[94] Box G.E.P.C., D.R., An Analysis of Transformations, *Journal of the Royal Statistical Society. Series B.*, **26(2)**: 211-252 (1964).

[95] Bruns R.E.S., I.S.; Neto B.B, Statistical Design - Chemometrics, *1st ed ed.*, **25**: Amsterdam,The Netherlands: Elsevier *Science*. 422 (2006).

[96] Elazazy M.S., In Factorial Design And Machine Learning Strategies: Impacts On Pharmaceutical Analysis. In Spectroscopic Analyses-Developments And Applications, E. Sharmin, Zafar, F., Editor. 2017, IntechOpen: London,UK. 213-230.

[97] Abbasi S., The Degradation Rate Study of Methyl Orange Using MWCNTs@TiO2 as Photocatalyst, Application of Statistical Analysis Based on Fisher's F Distribution, *Journal of Cluster Science*, **33** (2022).

[98] Fu H., Zhao P., Xu S., Cheng G., Li Z., Li Y., Li K., Ma S., Fabrication of Fe3O4 and Graphitized Porous Biochar Composites for Activating Peroxymonosulfate to Degrade p-Hydroxybenzoic Acid: Insights on the Mechanism, *Chemical Engineering Journal*, **375**: 121980 (2019).

[99] Ma W., Wang N., Fan Y., Tong T., Han X., Du Y., Non-Radical-Dominated Catalytic Degradation of Bisphenol A by ZIF-67 Derived Nitrogen-Doped Carbon Nanotubes Frameworks in the Presence of Peroxymonosulfate, *Chemical Engineering Journal*, **336**: 721-731 (2018).

[100] Zhao C., Shao B., Yan M., Liu Z., Liang Q., He Q., Wu T., Liu Y., Pan Y., Huang J., Wang J., Activation of Peroxymonosulfate by Biochar-Based Catalysts and Applications in the Degradation of Organic Contaminants: A Review, *Chemical Engineering Journal*, **416**: 128829 (2021).

[101] Fu H., Ma S., Zhao P., Xu S., Zhan S., Activation of Peroxymonosulfate by Graphitized Hierarchical Porous Biochar and MnFe2O4 Magnetic Nanoarchitecture for Organic Pollutants Degradation: Structure Dependence and Mechanism, *Chemical Engineering Journal*, **360** (2018).

[102] Su S., Guo W., Leng Y., Yi C., Ma Z., Heterogeneous Activation of Oxone by CoxFe3-xO4 Nanocatalysts for Degradation of Rhodamine B, *Journal of hazardous materials*, **244** (2012).

[103] Yao Y, Cai Y, Lu F, Wei F, Wang X, Wang S., Magnetic Recoverable MnFe2O4 and MnFe2O4-Graphene Hybrid as Heterogeneous Catalysts of Peroxymonosulfate Activation for Efficient Degradation of Aqueous Organic Pollutants, *Journal of Hazardous Materials*, **270**: 61–70 (2014).

[104] Johnson R.L., Tratnyek P.G., Johnson R.O.B., Persulfate Persistence under Thermal Activation Conditions, *Environmental Science & Technology*, **42(24)**: 9350-9356.

[105] Jiang S.F., Ling L.L., Chen W.J., Liu W.J., Li D.C., Jiang H., High Efficient Removal of Bisphenol A in a Peroxymonosulfate/Iron Functionalized Biochar system, Mechanistic Elucidation and Quantification of the Contributors, *Chemical Engineering Journal*, **359**: 572-83 (2019).

[106] Abbasi S., Improvement of Photocatalytic Decomposition of Methyl Orange by Modified MWCNTs, Prediction of Degradation Rate Using Statistical Models, *ournal of materials science: Materials in electronics*, **32(11)**:14137-48 (2021).

[107] Abbasi S., Hasanpour M., Variation of the Photocatalytic Performance of Decorated MWCNTs (MWCNTs-ZnO) with pH for Photo Degradation of Methyl Orange, *Journal of Materials Science: Materials in Electronics*, **28** (2017).

[108] Madjene F., Danane F., Chergui A., Trari M., Biosorption of Cr(VI) Ions onto Walnut Flowers: Application of Isotherm Models, *Iranian Journal of Chemistry and Chemical Engineering*, **41(12)** (2022).

[109] Qi C., Liu X., Ma J., Lin C., Li X., Zhang H., Activation of Peroxymonosulfate by Base: Implications for the Degradation of Organic Pollutants, Chemosphere, **151**: 280-288 (2016).

[110] Zhou Y., Jiang J., Gao Y., Ma J., Pang S.Y., Li J., Lu X.T., Yuan L.P., Activation of Peroxymonosulfate by Benzoquinone: A Novel Nonradical Oxidation Process, *Environmental Science & Technology*, **49(21)**: 12941-12950 (2015).

[111] Coltre D.S., Cionek C.A., Meneguin J.G., Maeda C.H., Braga M.U., de Araújo A.C., Gauze G.D., de Barros M.A., Arroyo P.A., Study of Dye Desorption Mechanism of Bone Char Utilizing Different Regenerating Agents, SN Applied Sciences, **2(12)**: 2150 (2020).

[112] Zeng L., Zhe F., Wang Y., Zhang Q., Zhao X., Hu X., Wu Y., He Y., Preparation of Interstitial Carbon Doped BiOI for Enhanced Performance in Photocatalytic Nitrogen Fixation and Methyl Orange Degradation, *J Colloid Interface Sci.*, **539**: 563-574 (2019).

[113] Yang S., Yang X., Shao X., Niu R., Wang L., Activated Carbon Catalyzed Persulfate Oxidation of Azo Dye Acid Orange 7 at Ambient Temperature, *Journal of hazardous materials*, 2011. **186(1)**: 659-666.

[114] Wang S., Wang J., Activation of Peroxymonosulfate by Sludge-Derived Biochar for the Degradation of Triclosan in Water and Wastewater, *Chemical Engineering Journal*, **356** (2018).

[115] Bennedsen L.R., Muff J., Søgaard E.G., Influence of Chloride and Carbonates on the Reactivity of Activated Persulfate, *Chemosphere*, **86(11)**: 1092-7 (2012).

[116] Rezaei R., Mohseni M., Impact of Natural Organic Matter on the Degradation of 2,4-Dichlorophenoxy Acetic Acid in a Fluidized Bed Photocatalytic Reactor, *Chemical Engineering Journal*, **310**: 457–463 (2017).

[117] Florenza X., Solano A.M., Centellas F., Martínez-Huitle C.A., Brillas E., Garcia-Segura S., Degradation of the Azo Dye Acid Red 1 by Anodic Oxidation and Indirect Electrochemical Processes based on Fenton's Reaction Chemistry, *Relationship between decolorization, mineralization and products. Electrochimica Acta*, **142**: 276-288 (2014).

[118] Thomas S., Abraham S.V., Aravind U.K., Aravindakumar C.T., Enhanced Degradation of Acid red 1 Dye Using a Coupled System of Zero Valent Iron Nanoparticles and Sonolysis, *Environ Sci Pollut Res Int*, **24(31)**: 24533-24544 (2017).

[119] Luo S., Wei Z., Dionysiou D.D., Spinney R., Hu W.P., Chai L., Yang Z., Ye T., Xiao R., Mechanistic Insight into Reactivity of Sulfate Radical with Aromatic Contaminants through Single-Electron Transfer Pathway, *Chemical Engineering Journal*, **327**: 1056-1065 (2017).

[120] Merga G., Aravindakumar C.T., Rao B.S., Mohan H., Mittal J.P., Pulse Radiolysis Study of the Reactions of $SO^{\cdot}-4$ with Some Substituted Benzenes in Aqueous Solution, *Journal of the Chemical Society, Faraday Transactions*, **90(4)**: 597-604 (1994).

[121] Vega E., Valdes H., New evidence of the Effect of the Chemical Structure of Activated Carbon on the Activity to Promote Radical Generation in an advanced Oxidation Process Using Hydrogen Peroxide, *Microporous and Mesoporous Materials*, In Press (2017).

[122] Liu G., Li C., Stewart B.A., Liu L., Zhang M., Yang M., Lin K., Enhanced Thermal Activation of Peroxymonosulfate by Activated Carbon for Efficient Removal of Perfluorooctanoic Acid, *Chemical Engineering Journal*, **399**: 125722 (2020).

[123] Trellu C., Oturan N., Keita F.K., Fourdrin C., Pechaud Y., Oturan M.A., Regeneration of Activated Carbon Fiber by Electro-Fenton Process, *Environmental Science & Technology*, **52** (2018).

[124] Yu J., Tang L., Pang Y., Zeng G., Feng H., Zou J., Wang J., Feng C., Zhu X., Ouyang X., Tan J., Hierarchical Porous Biochar from Shrimp Shell for Persulfate Activation: A Two-Electron Transfer Path and Key Impact Factors, *Applied Catalysis B: Environmental*, **260**: 118160 (2019).

[125] Chen J., Hong W., Huang T., Zhang L., Li W., Wang Y., Activated Carbon Fiber for Heterogeneous Activation of Persulfate: Implication for The Decolorization of Azo Dye, *Environmental Science and Pollution Research*, **23**: 18564-18574 (2016).

[126] Wang, S., J. Wang, Activation of Peroxymonosulfate by Sludge-Derived Biochar for the Degradation of Triclosan in Water and Wastewater, *Chemical Engineering Journal*, **356**: 350-358 (2019).

[127] Saputra E., Muhammad S., Sun H., Wang S., Activated Carbons as Green and Effective Catalysts for Generation of Reactive Radicals in Degradation of Aqueous Phenol, *RSC Advances*, **3(44)**: 21905-21910.

[128] Zhang J., Shao X., Shi C., Yang S., Decolorization of Acid Orange 7 with Peroxymonosulfate Oxidation Catalyzed by Granular Activated Carbon, *Chemical Engineering Journal*, **232**: 259-265 (2013).

[129] Huang ZhiYan H.Z., Wang TengLu W.T., Shen MinXian S.M., Huang ZhuJian H.Z., Chong YunXiao C.Y., Cui LiHua C.L., Coagulation Treatment of Swine Wastewater by the Method of in-Situ Forming Layered Double Hydroxides and Sludge Recycling for Preparation of Biochar Composite Catalyst, *Chemical Engineering Journal*, **369**: 784-792 (2019).

[130] Hu W., Xie Y., Lu S., Li P., Xie T., Zhang Y., Wang Y., One-Step Synthesis of Nitrogen-Doped Sludge Carbon as a Bifunctional Material for the Adsorption and Catalytic Oxidation of Organic Pollutants, *Science of The Total Environment*, **680**: 51-60 (2019).